5. Formulation Design, Development and *In-vitro* Cell Culture Studies

5.1 Introduction

Delivery of therapeutic agents to the brain is extremely challenging due to the existence of barriers such as blood-brain barrier (BBB), blood-cerebrospinal fluid (CSF) barrier and blood-spinal cord barrier. The anatomy of the BBB comprises the tight junction that seals together with the endothelial cell of brain capillaries along with a basement membrane [1,2]. BBB is primary and crucial obstacle for a molecule to transport into the brain parenchyma, as its function is to defend the entry of foreign substances from blood into brain tissue. Hence to overcome these hurdles it is essential to design and develop a very effective delivery system which can overcome the bioavailability related issues of drugs [1,3]. Nanoparticulate drug delivery systems are being extensively explored by the researchers to enhance the drug permeation across the brain thereby resulting in reduced dose, toxicity etc. [4–6]. Several approaches have been reported to enhance the brain uptake of acetylcholinesterase inhibitors including nanocarrier delivery systems like solid lipid nanoparticles, liposomes and polymeric nanoparticles which have attracted a significant interest [6–8]. Moreover, nanoparticulate delivery systems are having various advantages like prolonged and controlled release with selective biodistribution, dose reduction, protection of encapsulated drug from degradation and reduce side effects [8–12]. By considering these, nano-carrier delivery systems can result in reducing the cost and exhibits better patient compliance.

Although, donepezil (DNP) is 100% bioavailable, only 15-20% of the drug molecule reaches to the brain. Therefore, to maintain therapeutic concentration levels in the brain, DNP is administrated at higher doses which ultimately results in adverse effects [13,14]. Our objective in this study was to design and develop a suitable lipoprotein based DNP nano-carrier system for effective targeting to the brain, that might result in dose reduction and enhanced therapeutic efficacy of the molecule. Herein, we have selected to design a polymeric nanoparticles surface coated with a lipoprotein for improved brain upregulation and amyloid beta (Aβ) clearance by oral route. A lipoprotein (ApoE3) based nanocarriers exhibited a promising ability to improve brain uptake, binding to Aβ with high affinity and accelerating its clearance [15,16]. Nanocarrier systems have been proved for their targeted delivery, which leads to potential reduction in dose and its associated side effects [4,17–19]. Polymeric nanoparticles showed better tissue permeability and stability however, their utility is limited by scale up issues, biodegradation and toxicity. In the previous studies, PLGA loaded donepezil microparticles were prepared and characterized in order to achieve a sustained release formulation [20,21]. Self-assembled polymeric nanoparticles

composed of biodegradable amphiphilic block copolymers have emerged out as an attractive approach. Destabilizing effect on amyloid fibril formation and the ability to cross blood brain barrier has been investigated on DNP loaded PLGA-b-PEG nanoparticles [22]. Several reports have concluded that, the existence of PEG units promotes the long-circulating nature of polymeric nanoparticles which may interact with the Aβ peptide in the *in vitro* and *in vivo* conditions [6,23]. Amphiphilic block copolymers also have a hydrophilic corona, which could result in the formation of stealth properties and colloidal stability. Moreover, polymeric nanoparticles are an excellent nanocarriers which can easily be altered by surface modifications for targeting and better therapeutic efficacy. In addition, methoxy poly(ethyleneglycol)-polycaprolactone (mPEG-PCL) has a tendency to avoid nanoparticle uptake by phagocytic cells in the liver and can significantly reduce the gastric mucosal irritations [24,25]. Herein, our aim is to enhance the brain uptake of DNP by designing nanoparticles using in-house synthesized amphiphilic co-block polymer (mPEG-PCL) which is biodegradable and biocompatible. Further, these nanoparticles were thoroughly characterized and the optimized formulations were evaluated for *in vitro* cellular toxicity, cellular uptake, *in vivo* pharmacokinetic, biodistribution and therapeutic efficacy in Alzheimer induced animal model.

5.2 Experimentation

5.2.1 Materials

DNP and loratadine were kind gift samples of Vasudha Pharma Chem Limited (Hyderabad, India). HPLC grade solvents methanol, acetonitrile, dimethylformamide, dichloromethane, hexane and isopropyl alcohol were procured from Merck Millipore (MA, U.S.A.). Coomassie brilliant blue G dye and phosphate buffered saline; pH 7.4 (PBS) were procured from Himedia (Mumbai, India). Ammonium formate, methoxy Poly(ethylene glycol) (Mn, 5000), tin(II) 2-ethylhexanoate, ε-Caprolactone, trehalose, polysorbate 80, pepsin, acetyl thiocholine, ApoE3, 5,5'-Dithiobis-(2-Nitrobenzoic Acid) (DTNB), methylthiazolyldiphenyl-tetrazolium bromide (MTT), amyloid-beta protein fragment 1-42 and proteinase K were attained from Sigma Aldrich (St. Louis, MO, U.S.A.). Solid-Phase cartridges (Clearnert PEP-3 SPE) were procured from Agela Technologies (Wilmington, U.S.A.). Ultrapure water was acquired from Milli-Q system (Merck Millipore, MA, U.S.A.). Dialysis tubing (3.5 kDa) was procured from Thermo Fischer scientific (Rockford, U.S.A.). Polystyrene standards were purchased from Waters (U.S.A.). Fetal bovine serum (FBS), dulbecco's modified Eagle's medium high glucose (DMEM) and penicillin–streptomycin solution

were purchased from Gibco Life Technologies (U.S.A.). Dried toluene, triethylamine, cobalt nitrate hexahydrate, ammonium thiocyanate, bovine serum albumin (BSA), sodium chloride, monobasic potassium phosphate, sodium hydroxide, pancreatin, sodium phosphate, benzyl alcohol, dimethyl sulfoxide (DMSO) and diethyl ether were procured from SISCO research laboratories (SRL, India). Thioflavin T and 1,1,1,3,3,3-Hexafluoro-2-propanol (HFIP) were obtained from Tokyo Chemical Industry Co., Ltd. (Tokyo, Japan).

5.2.2 Instruments / Equipments

Ultrasonic microtip processor (500W; 20 KHz, Vibra-Cell™, Sonics®, USA) and magnetic stirrer with a hot plate and temperature controller (Tarsons, India or Remi, India) was used in the preparation of nanoparticles. Rota vacuum evaporator (Rotavapor R210, Buchi, Switzerland) was utilized for the removal of organic solvents in the nano-formulations. Ultrasonic bath sonicator (Toshiba, India) and temperature-controlled centrifuge (Centrifuge CPR 24, Remi, India) was used in sample preparation for the determination of percent entrapment efficiency and drug loading. Freezer (-20 ºC, Vestfrost, India) was used for freezing the nanoparticles prior to lyophilization process. Lyophilizer (Freezone 2.5, Labconco, USA) was utilized for the freeze drying of the nanoparticles. Malvern Zetasizer (Zetasizer nanoZS, ZEN3600, Malvern, UK) was utilized for characterization of average particle size and zeta potential. Thermal analysis was carried out by differential scanning calorimeter (DSC-60plus, Shimadzu, Japan). Morphological characterization of nanoparticles was estimated by utilizing field emission scanning electron microscopy (FESEM, Apreo S with Xt microscope control version 13.5.0, FEI limited, USA) and high-resolution transmission electron microscope (HR-TEM, Technai G2, 200 kV, FEI, USA). For in vitro cell culture studies, CO_2 incubator (Thermo Scientific, USA), cell culture hood (India), inverted microscope (Zeiss, India), laboratory centrifuge (Thermo Scientific, USA) and microplate reader (Bio Tek ELX50, Epoch) was utilized.

5.2.3 Synthesis of Amphiphilic Di-block polymer

Methoxy polyethylene glycol (M ~5000 Da, 1 g, 0.2 mmol) was solubilized in dried toluene. ε-caprolactone (131.41 equivalent, 3.0 g, 26.28 mmol) was added dropwise to the above solution in Schlenk tube, later tin (II) 2-ethylhexanoate (10 mol % of initiator, 15 µL) was mixed and reaction was processed under nitrogen atmosphere for about 24 h at 120°C (Fig. 5.1). Reaction mixture was further concentrated by utilizing rotary evaporator, product was solubilized in dichloromethane and precipitated two times by chilled methanol and third time with chilled diethyl ether [24,25].

Polymer was properly dried and evaluated by using ^{1}H-NMR (Bruker, Germany) and gel permeation chromatography (GPC) (Waters, U.S.A., Styragel HR column). The polymeric sample was dissolved in dimethylformamide at a concentration of 5mg/mL, filtered using 0.4µ syringe filter. Average molecular weight of the polymer was calculated by GPC equipped with Waters 2414 RI detector.

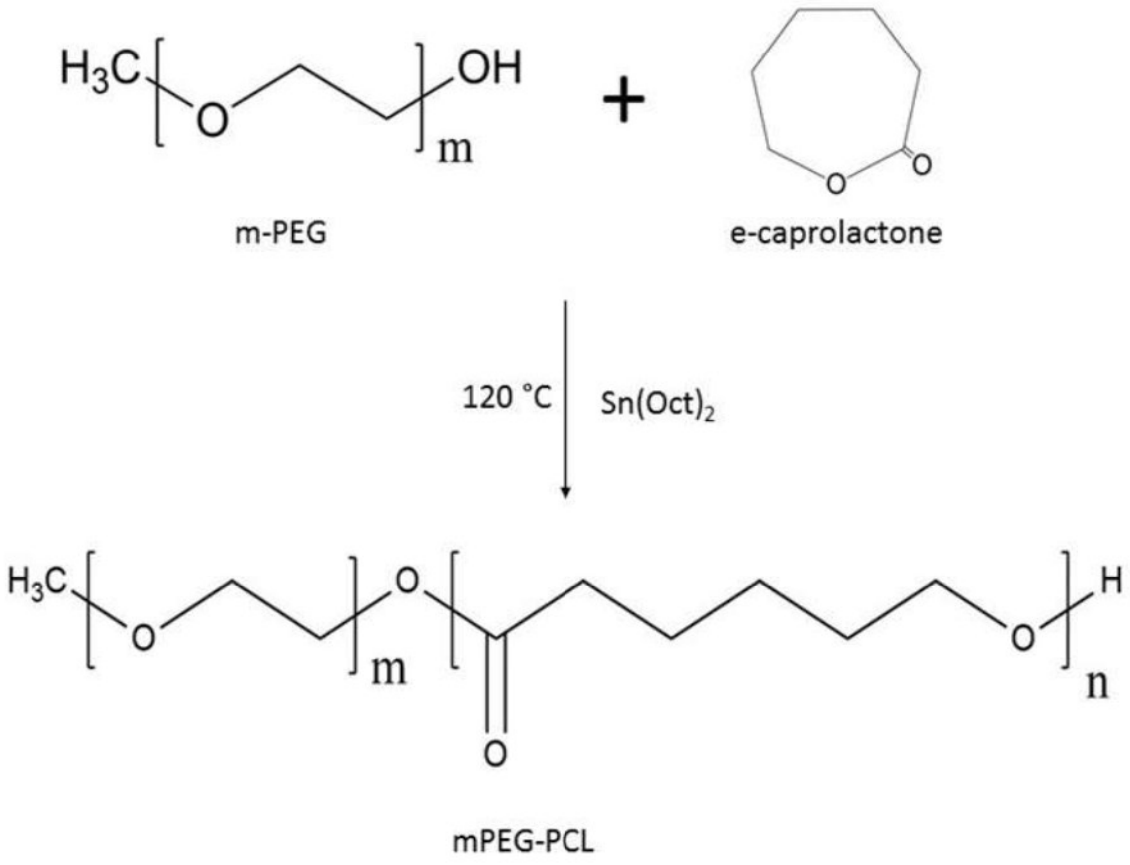

Fig. 5.1 Scheme for polymer synthesis

5.2.4 Formulation of polymeric nanoparticles

The criteria for the selection of preparation technique is based on the potential of polymer to encapsulate DNP. Initially, we have tried with all possible techniques like film hydration method, solvent emulsification and nano-precipitation method [26–29]. Based on the results obtained, we have selected appropriate method for the preparation of nanoparticles.

Polymeric nanoparticles were formulated by utilizing nanoprecipitation method [30,31]. Briefly, 12.5 mg of polymer, 5 mg of DNP and 1.6 µL of triethylamine (equimolar of donepezil hydrochloride) were solubilized in 1.8 mL of acetonitrile (organic phase) followed by dropwise addition to 5 mL of Milli-Q water (aqueous phase) under stirring for 20 min. The resulting nano-

dispersion was dialyzed with purified water for 8 h by dialysis tubing (molecular weight cut off - MWCO, 3.5 k Da) to remove unentrapped drug. Water was replaced twice in the course of dialysis.

5.2.5 Optimization of polymeric nanoparticles by central composite design

A central composite design (CCD) was utilized to obtain the minimum number of experiments required to optimize the DNP loaded polymeric nanoparticles using Design-Expert (Version 8.0.7.1, Stat-Ease Inc., Minneapolis, MN, USA) [30,32,33]. Based on preliminary batches, the drug:polymer ratio (A, w/w) was altered from 0.1 to 0.9 and solvent:non-solvent ratio (B, v/v) was altered from 0.02 to 0.48, opted as independent variables. As proposed by the design, a total thirteen runs were executed for particle size (Y1), polydispersity index (Y2) and %drug loading (Y3) as the response (dependent) variables (Table 5.1 & 5.2). Five center points were selected to estimate the reliability of the design. This design gives information about the interaction effects of independent variables and its formulation characteristics. Analysis of variance for all the responses were executed and the best fit model was statistically selected based on various parameters like multiple correlation coefficient (R^2), adjusted and predicted correlation coefficients, standard deviation and coefficient of variance. Graphically, 3D response surface plots were generated by software. The significance level was considered at p-value < 0.05. The optimized nano-formulation (D1-NPs) was prepared according to the predictor profile for greater desirability to attain targeted goal within the design space. The influence of each independent variable on responses was detected using CCD. Moreover, the model optimization was executed on the basis of achieving lowest particle size and PDI with higher % drug loading.

Table 5.1: Levels of Independent factors used in the design

Factor Code	Independent Factor	Levels				
		-1.414	**-1**	**0**	**1**	**1.414**
A	Drug:Polymer ratio (w/w)	0.1	0.25	0.5	0.75	0.9
B	Solvent:Non-Solvent ratio (v/v)	0.02	0.1	0.25	0.4	0.48

Table 5.2: Central Composite Design for the optimization of nano-formulation

Formulation Code	Drug:Polymer ratio (w/w)	Solvent:Non-Solvent ratio (v/v)
F1	0.1	0.25
F2	0.25	0.4
F3	0.25	0.1
F4	0.5	0.25
F5	0.5	0.25
F6	0.5	0.25
F7	0.5	0.25
F8	0.5	0.25
F9	0.5	0.02
F10	0.5	0.48
F11	0.75	0.1
F12	0.75	0.4
F13	0.9	0.25

The optimized formulation was evaluated with several cryoprotectants to find out the best using Freeze Dry System (LabConco®) for 48 h. The lyophilized nano-formulation was then reconstituted by adding Milli-Q water followed by gentle agitation. The dispersed nano-formulation was evaluated for redispersibility index (Sf/Si, ratio between particle size later and earlier lyophilization), if the value is lower than two then the selected cryoprotective system was found to be efficient. Further the residual organic solvent content in the lyophilized nano-formulation was estimated by headspace gas chromatography. As per the procedure organic solvents used were acetonitrile and triethyl amine. The benzyl alcohol was selected as a sample diluent due to the reproducibility, higher solubility and best baseline with no interference at the retention times of the residual organic solvents of interest. The GC system consisted of Shimadzu GC-2010 Plus equipped with FID detector and Shimadzu HS-10 auto sampler was used for sample analysis Column used for the analysis was Rtx-624 (30 m X 0.32 mm ID X 1.8 µm) capillary column. Samples were prepared by solubilizing about 500 mg of lyophilized formulation with 5 mL of extracting solvents in a 20-mL headspace GC vial. Other chromatographic conditions are tabulated as below Table 5.3.

Table 5.3 Gas Chromatography operating conditions

Instrument Details	:	Shimadzu GC-2010 Plus with HS-10 Injector		
Column Details	:	Rtx-624 (30 m X 0.32 mm ID X 1.8 µm)		
Injection Mode	:	Split		
Injection Port Temp	:	180°C		
Total Flow	:	91.5 mL/min		
Column Flow	:	1.50 mL/min		
FID Temp.	:	260°C		
Carrier gas	:	Nitrogen		
Column Oven program	:	Rate	Temp. (°C)	Hold Time (min)
		-	50.0	6.00
		50.00	220.0	8.00
		HS-10 Parameters		
Oven Temp	:	95.0 °C		
Sample Line Temp	:	110.0 °C		
Transfer Line Temp	:	120.0 °C		
Equilibrium Time	:	30.00 min		
Injection Time	:	1.00 min		
Run Time	:	17.40 min		
GC Cycle Time	:	23.00 min		

5.2.6 Surface coating of optimized nanoparticles by polysorbate-80

Surface coating of optimized nanoparticles by polysorbate-80 was performed to enhance the brain uptake (D2-NPs) [34–37]. In brief, lyophilized nanoparticles were dispersed in water consisting 1% of polysorbate-80 (20 mg/mL of nanoparticles). This was further bath sonicated for 10 min for complete dispersion of nanoparticles and then incubated for about 30 min at normal room temperature. The quantification of surface coating was performed as per reported methods by colorimetric method using ammonium thiocyanate and cobalt nitrate hexahydrate [34].

5.2.7 ApoE3 conjugation with coated nanoparticles

The ApoE3 (20µg/mL) was finally adsorbed to the lyophilized surface coated nanoparticles by stirring for 1 h at room temperature and further bath sonicated for 10 min (D3-NP) [38,39]. Quantification of ApoE3 conjugation efficiency was determined as per previously reported methods by Bradford assay utilizing Coomassie brilliant blue G dye [40].

5.2.8 Characterization of nanoparticles

(a) Particle size distribution and zeta potential

The mean particle size, poly dispersity index and zeta potential of nanoparticles were estimated by utilizing Zetasizer (nanoZS, Malvern, UK). The samples were diluted approximately with ultrapure water, filled in disposable polystyrene cells and analyzed at a scattering angle of 173°. Morphology of the polymeric nanoparticles was assessed by field emission scanning electron microscopy (FE-SEM) (Apreo LoVac, FEI, U.S.A.) and transmission electron microscope (HR-TEM) (Technai G2, 200 kV, FEI, U.S.A.). Prior to analysis, 100 µL of polymeric nanoparticles dispersion was placed on a cover slip and dried overnight under vacuum. Later gold sputter coated using gold sputter module in a high vacuum evaporator (Quorum:ES; Quorum technologies, UK). The gold coated samples were then scanned.

(b) Drug loading and entrapment efficiency

For the estimation of drug loading, known quantity of lyophilized nanoparticles was transferred to a 15 mL centrifugal tube and disrupted by adding sufficient amount of acetonitrile and keeping the same in ultrasonic bath for 10 min at 25 ºC for complete release of drug from the nanoparticle system. This was followed by centrifugation at 5000 rpm and the supernatant was analyzed by in-house developed HPLC method after dilution as reported in Chapter 3.

Polymeric nanoparticles were separated from the dispersion by centrifuging at 20,000 rpm for about 1 h for the estimation of entrapment efficiency. The separated nanoparticles were washed with water to remove any traces of drug adsorbed over the surface of nanoparticles and the dispersion was centrifuged again. The separated nanoparticles were disrupted by adding sufficient amount of acetonitrile and keeping the same in ultrasonic bath for 10 min at 25 ºC for complete release of drug from the nanoparticle system. The supernatant was obtained by centrifugation at 5000 rpm and it was analyzed by in-house developed HPLC method after dilution as reported in Chapter 3. Analysis was carried out in triplicate and reported as mean with standard deviation.

Loading efficiency and entrapment efficiency of DNP in nanoparticles was measured by using the following formulae.

$$\text{Loading efficiency (\%)} = \frac{\text{Weight of DNP in polymeric nanoparticles}}{\text{Weight of polymeric nanoparticles}} \text{X } 100$$

$$\text{Entrapment efficiency (\%)} = \frac{\text{Amount of DNP in polymeric nanoparticles}}{\text{Amount of DNP taken in prepartion of polymeric nanoparticles}} \text{X } 100$$

(c) Protein binding assay

Polymeric nanoparticles were evaluated for its protein binding efficiency using Biuret assay as per reported methods [41]. Briefly, 10 mg of polymeric nanoparticles were incubated with 4 % BSA in 10 mL and placed in an orbital shaking incubator for about 24 h at 120 rpm. The nanoparticular suspension was centrifuged at 15000 rpm, biuret reagent (4 mL) was added to the supernatant (1mL) and incubated for 30 min in orbital shaker at 120 rpm. Further, supernatant was analyzed by UV spectrophotometry (Shimadzu UV-1800) at 540 nm for unabsorbed protein content. The standard calibration curve for BSA was plotted in the range of 500 to 2500 µg/mL which is used for quantification [30].

(d) *In vitro* release studies

The *in-vitro* release for all the formulations viz, D1-NPs, D2-NPs and D3-NPs were investigated in phosphate buffered saline (PBS, 0.1 M) pH 7.4, under sink conditions using dialysis membrane method. Briefly, pure drug solution and all the formulations (equivalent to 1 mg of DNP, n=3) were wrapped in a dialysis membrane (MWCO 3.5 kDa) and dialyzed against 100 mL of PBS (pH 7.4). The samples were maintained at 37°C in orbital shaking incubator at 120 rpm. At selected time intervals (0.25, 0.5, 1, 2, 4, 6, 9, 12, 18, 24, 36, 48, 72 and 96 h), 1mL aliquots of the medium were withdrawn followed by replacement of same volume with the fresh release medium. All the samples were filtered and analyzed by using in-house developed and validated HPLC method as described in Chapter 3 [42]. The percent cumulative drug release was calculated and the obtained data was evaluated by mathematical modeling [43–45]. The modeling of release data was assessed by several kinetic models like zero order, first order, Higuchi, Korsmeyer–Peppas and Hixon Crowell to determine the possible mechanism of drug release.

Zero order equation: $F = k_0.t$

First order equation: $F = 100\ (1\text{-}e^{-k_1.t})$

Higuchi equation: $F = k_H.t^{0.5}$

Korsmeyer–Peppas equation: $F = k_{KP}.t^n$

Hixon Crowell equation: $F = 100\ [1-(1-k_{HC}.t)^3]$

In all these models, F is the fraction percentage of drug released in time t; k_0 is the zero order rate constant; k_1 is the first order rate constant; k_H is the higuchi release constant; k_{KP} is the korsmeyer–peppas release constant incorporating geometric and structural features of the formulations; n is the diffusional exponent representing the drug release mechanism; k_{HC} is the release constant in Hixon Crowell model. For spherical particles the value of n=0.43 indicated Fickian diffusion; values between 0.43 and 0.85 ($0.43 < n < 0.85$) indicate non- Fickian diffusion, the value of n is equal to 0.85 in case of zero order release (case II transport) and $n > 0.85$ for super case II transport. Best fit model and release mechanism were identified on the basis of highest regression values of correlation coefficients for the release data.

(e) Thermal studies

DSC analysis of the nano-formulations were conducted by utilizing DSC-60 plus (Shimadzu, Kyoto, Japan) [37]. The sample preparation was similar as mentioned in Chapter 4. The respective thermograms of the formulations were corelated with the pure drug and other excipients used in the formulation design.

(f) Stability studies

(i) Stability of polysorbate-80 coated and ApoE3 conjugated polysorbate-80 coated nanoparticles in simulated gastric fluid (SGF) and simulated intestinal fluid (SIF)

Stability in SGF and SIF is one of the key concerns which may alter the *in vivo* parameters of the nano-formulations. The stability studies of D2-NPs and D3-NPs in SGF and SIF were carried out as per previously reported method [34]. In brief, 200 µL of D2-NPs and D3-NPs were incubated with 1800 µL of respective fluids for 2h in SGF while 6hr in SIF and the influence on particle size, PDI, % EE and the intactness of surface coating were determined.

(ii) Long-term stability of lyophilized formulation

The long-term stability studies for all the formulations were performed as per the International Council for Harmonization (ICH, Q1A, R2) [30,46]. Lyophilized polymeric nanoparticles were placed in the stability chamber at 25 ± 2 °C, 60 ± 5% RH for 3 months. All formulations were monitored for its size, PDI, % EE and zeta potential after 1, 2, and 3 months. Further, the degradation rate constant was determined.

5.2.9 *In vitro* amyloid beta$_{1-42}$ fibrillation study

(a) Aβ$_{1-42}$ sample preparation

Aβ$_{1-42}$ sample solution was prepared as per earlier reported methods [47–51]. In brief, lyophilized Aβ$_{1-42}$ peptide was solubilized in HFIP to get a concentration of 1 mg/mL, resulting solution was bath sonicated for about 10 min and later incubated at 4 ºC under shaking for 2 h. Further, this solution was divided into different aliquots into a microcentrifuge tubes and stored at -20 ºC after evaporating HFIP solvent from the samples by applying gentle stream of nitrogen gas. Prior to use, these dry aliquot samples were resuspended with anhydrous DMSO to get a concentration of 1 mM followed by bath sonication for about 10 min and then diluted to the required concentration by using PBS (pH 7.4; 10mM). This prepared solution was immediately used for performing the below experiments.

(b) Thioflavin T fluorescence assay for fibril inhibition of Aβ$_{1-42}$ peptide

To estimate the fibril inhibition, Aβ$_{1-42}$ monomeric solution was incubated with or without pure drug, D1-NPS, D2-NPs and D3-NPs in 1.5 mL centrifugal tubes at 37 ºC for 24 h. The final concentration of Aβ$_{1-42}$ was maintained at 25 µM in the sample mixtures. To investigate the Aβ fibril formation process, sample aliquots were collected from the mixture at pre-determined time intervals for analysis. Further, 100 µL of withdrawn samples were mixed with 200 µL of 20 µM ThT buffer solution (prepared in PBS, pH 7.4, 10 mM) and vortexed for about 10 min and analyzed using Horiba Fluorolog-3 spectrofluorometer. The samples were analyzed at an excitation and emission wavelengths of 440 nm and 485 nm respectively for measuring ThT fluorescence intensities. The experimenters were conducted in triplicate and all the data was represented in mean ± standard deviation. Further the data obtained from ThT fluorescence assay was fitted into a sigmoidal curve and the fibrillation growth rate has been derived by using the below equation;

$$Y = Y_i + \frac{Y_f + Y_i}{1 + e^{-(t - t_{1/2})k}}$$

$$\text{Lag time} = t_{1/2} - \frac{2}{k}$$

where Y is the time-dependent fluorescence intensity, Y_i and Y_f are the initial and final fluorescence intensities, k is the apparent first-order aggregation constant and $t_{½}$ is the time when the fluorescence intensities are half of the maximum one. The lag time is defined as refraction at the maximum fibrillation rate. The lag time is defined as the time of the refraction at the maximum fibrillation rate point, which is determined by using above equation.

(c) Proteolysis assay

$A\beta_{1-42}$ fibril solution was prepared by incubating 25 µM $A\beta_{1-42}$ monomer solution for 7 days at 37 ºC. DNP and its formulation samples were prepared by mixing with $A\beta_{1-42}$ monomer solution and incubated at same conditions as mentioned above. Further, the prepared samples were treated with proteinase K (100 µg/mL) for proteolysis and incubated at 37 ºC. The sample aliquots were collected from the mixture at selected time intervals for ThT fluorescence assay [48].

5.2.10 Cell culture studies

(a) Cell viability assay

The human liver hepatocellular carcinoma cells (HepG2), human glioblastoma cell line (U87) and human neuroblastoma cell line (SH-SY5Y) were acquired from National Centre for Cell Science (NCCS), Pune, India. Cells were maintained in T-25 cm^2 tissue culture flasks with DMEM supplemented with 100 units/mL penicillin, 100 µg/mL streptomycin and with 10% FBS. Moreover, for SH-SY5Y cells, Ham's F12 was also used. Cells were stored at 37°C in humidified 5% CO2 incubator. (Esco Incubators, India and Thermoscientific, USA).

The cell viability of pure drug, D1-NPS, D2-NPs and D3-NPs were measured by utilizing MTT cytotoxicity assay on all the cell lines. Briefly, the cells were sub cultured into sterile 96-well plate at a density of 5×10^3 cells per well. After incubation of the cultures for 24 h to allow the cells to reach 70-80 % confluence, cells were treated with varying concentration at a range of 50 - 500 µg/mL of DNP and incubated for 24 h. Further, the media was replaced with fresh media (150 µL) comprising 0.5mg/ml MTT dye and incubated for 4 h at 37 °C. The media was removed and 150 µL of DMSO solution was added to each well. The absorbance was estimated at 570 nm with reference wavelength at 630 nm using Tecan Infinite M200 microplate reader (Tecan, Switzerland) or Epoch microplate reader (BioTek, ELX 50, India). Percentage of cell viability was calculated as follows:

$$\text{Cell Viability (\%)} = \frac{\text{Absorbance of sample}}{\text{Absorbance of control}} \text{ X } 100$$

(b) Cellular uptake studies

To understand the cellular uptake of the developed formulations, human glioblastoma cell line (U87) and human neuroblastoma cell line (SH-SY5Y) was selected. Cultured cells were incubated with pure drug, D1-NPs, D2-NPs and D3-NPs at a concentration of 150 µg/mL (n=4) for selected time intervals (4, 6, 12 and 24 h) and the untreated cells were kept as control group. Further, media

was withdrawn and centrifuged at 1500 to remove any cell or debris. DNP was extracted as per our previously developed HPLC method as discussed in Chapter 3 [42]. Briefly, 50 µL of loratadine (internal standard) and 150 µL of 10 mM ammonium formate buffer will be added to the media and followed by solid phase extraction. Further, samples were analyzed by using HPLC as discussed in Chapter 3.

(c) Amyloid beta$_{1-42}$ induced neuronal toxicity in cell lines

To study the efficacy of the developed formulations, Aβ_{1-42} induced neurotoxic SH-SY5Y cell model was used. After incubation of SH-SY5Y cells for 24 h with 25 µM Aβ_{1-42}, cells were treated with pure drug, D1-NPs, D2-NPs and D3-NPs at a concentration of 50 and 150 µg/mL for 24 h. Then the cell viability was estimated by using MTT assay as described above.

5.3. Results and Discussion

5.3.1 Synthesis and characterization of amphiphilic di-block copolymers

mPEG-PCL was synthesized by simple ring opening polymerization reaction of ε-caprolactone by utilizing tin(II) 2-ethylhexanoate as a catalyst. The ^{1}H-NMR data confirmed the synthesis of mPEG-PCL di-block copolymer (Fig. 5.2). As per ^{1}H-NMR spectrum, presence of peaks at δ 1.39, 1.66, 2.32 and 4.07 represents formation of polycaprolactone and characteristic peaks at δ 3.66 and 3.39 indicates the presence of methylene units of PEG. Molecular weight of di-block copolymer was determined by ^{1}H-NMR and GPC. ^{1}H-NMR data represented molecular weight of polymer to be ~15207 Da whereas GPC data showed Mn and Mw of 12147 Da and 14955 Da respectively with molecular weight distribution of 1.98 (Fig. 5.3). Yield = 89%.

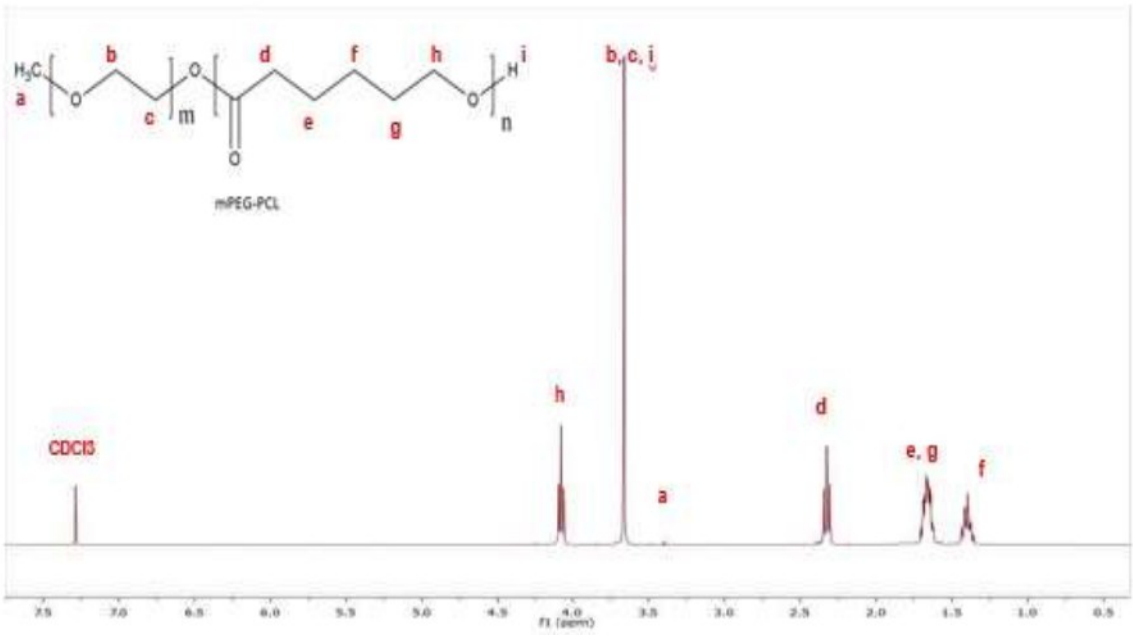

Fig. 5.2: H-NMR data of mPEG-PCL

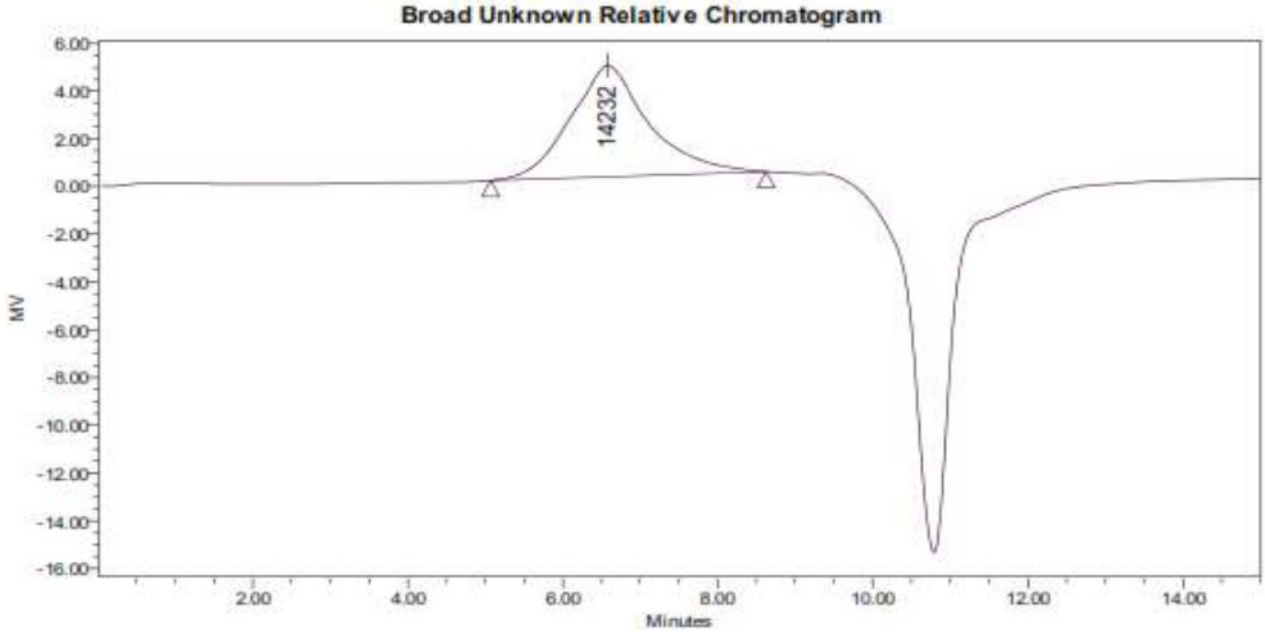

Broad Unknown Relative Peak Table

	Distribution Name	Mn (Daltons)	Mw (Daltons)	MP (Daltons)	Mz (Daltons)	Mz+1 (Daltons)	Polydispersity	Mz/Mw	Mz+1/Mw
1		11869	19099	14232	40758	99390	1.609204	2.134018	5.203844

Fig. 5.3: GPC data of mPEG-PCL

5.3.2 Formulation development

The synthesized polymer is amphiphilic in nature with methoxy polyethylene glycol as a hydrophilic and polycaprolactone as a hydrophobic moiety. Polyethylene glycol is used to enhance the blood circulation time in the body. Polycaprolactone is a biocompatible and biodegradable polymer which is metabolized into monomeric units of ε-caprolactone inside the body. Initially, we have screened with all different types of preparation techniques like film-hydration, solvent evaporation and nano-precipitation at different drug loading capacity. The suitable technique has been screened based on the maximum drug loading capacity and minimum particle size. Out of these methods we have observed maximum entrapment and lower particle size in case of nanoprecipitation method. And this technique is most widely utilized method for preparation of nanoparticles due to its capacity to achieve maximum entrapment efficiency. All the experiments were conducted in triplicate and the results are represented in mean ± standard deviation (Table 5.4).

Table 5.4 Different methods used for the fabrication of polymeric nanoparticles

Preparation technique	Theoretical Loading (%)	Average Particle Size (nm)	PDI*	% EE
Film Hydration	10	345.5 ± 9.54	0.44 ± 0.04	14.64 ± 4.58
Film Hydration	20	398.3 ± 2.21	0.47 ± 0.08	29.25 ± 5.15
O/W Emulsion	10	248.8 ± 3.48	0.22 ± 0.03	44.84 ± 6.92
O/W Emulsion	20	301.2 ± 5.21	0.31 ± 0.15	58.18 ± 2.54
Nanoprecipitation	10	98.1 ± 4.25	0.21 ± 0.09	70.52 ± 6.71
Nanoprecipitation	20	110.5 ± 1.42	0.19 ± 0.14	79.48 ± 5.33

5.3.3 Optimization of polymeric nanoparticles

The optimization process of polymeric nanoparticles was implemented by employing quality by design (QbD) approach. Moreover, it suggests the optimized batch using minimum number of trials by statistically varying process parameters. Response surface methodologies like Box-Behnken design and CCD and are generally explored for evaluating the variations between the variables. However, we have used CCD design for optimizing polymeric nanoparticles. Polymeric nanoparticulate system was developed by nanoprecipitate technique, that majorly depends on the quick diffusion of solvent over the interface between the polymer-solvent and aqueous phase. From

the preliminary studies, drug:polymer and solvent:non-solvent ratio showed significant effect on selected responses like mean particle size, PDI and % drug loading. Five levels of independent variables were selected and the results are described in Table 5.5. This design gives information about polynomial equations involved in interaction effects of independent variables and its responses. The validation of these polynomial equations produced by design expert software were evaluated statistically by using analysis of variance. Response surface plots generated were utilized to study the effects of the predesigned responses like particle size, PDI and % drug loading. The attentive observation of surface plots and polynomial equations results in understanding the influence of each variable individually and also in grouping with other variables on each response.

Table 5.5 Design and optimization of mPEG-PCL polymeric nanoparticles by nanoprecipitation technique

Independent Factors		**Responses** (Experimental values)			**Predicted Values**		
Drug:Polymer	**Solvent:Non-solvent**	**Particle Size (nm)**	**PDI**	**% DL***	**Particle Size (nm)**	**PDI**	**% DL***
0.1	0.25	85.52	0.17	7.15	86.70	0.15	9.72
0.25	0.4	121.48	0.22	16.15	126.49	0.23	16.70
0.25	0.1	187.25	0.17	11.28	178.57	0.19	11.64
0.5	0.25	99.65	0.27	15.87	103.06	0.24	16.11
0.5	0.25	102.79	0.26	16.48	103.06	0.24	16.11
0.5	0.25	96.87	0.21	15.36	103.06	0.24	16.11
0.5	0.25	104.47	0.25	16.12	103.06	0.24	16.11
0.5	0.25	109.75	0.23	17.07	103.06	0.24	16.11
0.5	0.02	343.94	0.39	16.87	354.89	0.38	16.59
0.5	0.48	234.52	0.34	22.78	227.61	0.34	22.25
0.75	0.1	348.22	0.52	17.15	338.46	0.51	17.53
0.75	0.4	220.58	0.44	19.28	224.52	0.42	19.85
0.9	0.25	290.51	0.55	17.33	293.04	0.57	16.94

*% DL = Drug Loading

I. Effect on particle size

The full quadratic model equations for particle size was generated by response surface regression process by utilizing design expert software. The software recommended the quadratic model, for

the particle size response based on the statistical significance and model maximizing the adjusted R^2 and the predicted R^2 (Table 5.6 & 5.7).

Table 5.6 Statistical parameters for model selection of particle size

Source	Sequential p-value	Lack of Fit p-value	Adjusted R-Squared	Predicted R-Squared
Linear	0.0471	< 0.0001	0.3488	0.0571
2FI	0.7573	< 0.0001	0.2845	-0.0795
Quadratic	**< 0.0001**	**0.1423**	**0.9949**	**0.9837¥**
Cubic	0.0523	0.6590	0.9978	0.9953

¥ suggested

Table 5.7 Analysis of variance table for response surface quadratic model of particle size

Source	Sum of Squares	df	Mean Square	F Value	Prob > F p-value
Model	110781.01	5	22156.20	469.19	< 0.0001¥
A-A	1021.60	1	1021.60	21.63	0.0023
B-B	32952.04	1	32952.04	697.80	< 0.0001
AB	672.62	1	672.62	14.24	0.0069
A^2	11511.05	1	11511.05	243.76	< 0.0001
B^2	55865.86	1	55865.86	1183.04	< 0.0001
Residual	330.56	7	47.22		
Lack of Fit	234.42	3	78.14	3.25	0.1423£
Pure Error	96.13	4	24.03		
Cor Total	111111.57	12			

Where, A: Drug:Polymer ratio (w/w), B: Solvent:Non-Solvent ratio (v/v), ¥ significant and £ not significant

The F-value of a model is 469.19 indicates that it is statistically significant. However, there is just a 0.01% probability that the "F-Value of a model" is this huge might arise because of noise. The estimations of "Prob > F" below 0.10 represents model values are significant. Moreover, in this instance A, B, AB, A^2, B^2 are significant model values. The estimations above 0.10 represents the model values are not significant and the "Lack of Fit F-value" of 3.25 indicates the Lack of Fit is not significant comparative to the pure error. Further, there is a 14.23% possibility that a "Lack of Fit F-value" this huge might arise because of noise.

Table 5.8 Summary of model fitting statistics for particle size

Fitting Statistics	
Standard deviation	6.87
Mean	179.66
Coefficient of variance (%)	3.82
PRESS	1811.40
R^2	0.9970
Adjusted R^2	0.9949
Predicted R^2	0.9837
Adequate Precision	56.67

The predicted R^2 of 0.9837 is in reasonable concurrence with the adjusted R^2 of 0.9949 (Table 5.8). Adequate precision estimates the signal to noise ratio. Ideally, a ratio more than 4 is desirable. Model ratio of 56.67 represents an adequate signal. Thus, this model might be utilized to explore the design space.

II. Effect on polydispersity index (PDI)

The full quadratic model equations for PDI was generated by response surface regression process by utilizing design expert software. The software recommended the quadratic model, for the PDI response based on the statistical significance and model maximizing the adjusted R^2 and the predicted R^2 (Table 5.9 & 5.10).

Table 5.9 Statistical parameters for model selection of PDI

Source	Sequential p-value	Lack of Fit p-value	Adjusted R-Squared	Predicted R-Squared
Linear	0.0005	0.0157	0.7334	0.6291
2FI	0.3527	0.0141	0.7323	0.6138
Quadratic	**0.0003**	**0.5391**	**0.9671**	**0.9252¥**
Cubic	0.3033	0.8446	0.9714	0.9730

¥ suggested

Table 5.10 Analysis of variance table for response surface quadratic model of PDI

Source	Sum of Squares	df	Mean Square	F Value	Prob > F p-value
Model	0.1935	5	0.0387	71.68	< 0.0001¥
A-A	0.0000	1	0.0000	0.01	0.9141

B-B	0.0058	1	0.0058	10.65	0.0138
AB	0.0042	1	0.0042	7.82	0.0266
A^2	0.0206	1	0.0206	38.08	0.0005
B^2	0.0228	1	0.0228	42.28	0.0003
Residual	0.0038	7	0.0005		
Lack of Fit	0.0015	3	0.0005	0.84	0.5391[£]
Pure Error	0.0023	4	0.0006		
Cor Total	0.1973	12			

Where, A: Drug:Polymer ratio (w/w), B: Solvent:Non-Solvent ratio (v/v), [¥] significant and [£] not significant

The F-value of a model is 71.68 indicates that it is statistically significant. However, there is just a 0.01% probability that the "F-Value of a model" is this huge might arise because of noise. The estimations of "Prob > F" below 0.10 represents model values are significant. Moreover, in this instance A, B, AB, A^2, B^2 are significant model values. The estimations above 0.10 represents the model values are not significant and the "Lack of Fit F-value" of 0.84 indicates the Lack of Fit is not significant comparative to the pure error. Further, there is a 53.91% possibility that a "Lack of Fit F-value" this huge might arise because of noise.

Table 5.11 Summary of model fitting statistics for PDI

Fitting Statistics	
Standard deviation	0.02
Mean	0.31
Coefficient of variance (%)	7.51
PRESS	0.01
R^2	0.9808
Adjusted R^2	0.9672
Predicted R^2	0.9253
Adequate Precision	26.18

The predicted R^2 of 0.9253 is in reasonable concurrence with the adjusted R^2 of 0.9672 (Table 5.11). Adequate precision estimates the signal to noise ratio. Ideally, a ratio more than 4 is desirable. Model ratio of 26.18 represents an adequate signal. Thus, this model might be utilized to explore the design space.

III. Effect on percent drug loading

The full quadratic model equations for % drug loading was generated by response surface regression process by utilizing design expert software. The software recommended the quadratic

model, for the PDI response based on the statistical significance and model maximizing the adjusted R^2 and the predicted R^2 (Table 5.12 & 5.13).

Table 5.12 Statistical parameters for model selection of % drug loading

Source	Sequential p-value	Lack of Fit p-value	Adjusted R-Squared	Predicted R-Squared
Linear	0.0059	0.0086	0.5706	0.1746
2FI	0.5351	0.0070	0.5439	0.1955
Quadratic	**0.0001**	**0.3994**	**0.9535**	**0.8848¥**
Cubic	0.9476	0.1297	0.9363	0.1196

¥ suggested

Table 5.13 Analysis of variance table for response surface quadratic model of % drug loading

Source	Sum of Squares	df	Mean Square	F Value	Prob > F p-value
Model	115.52	5	23.10	50.21	< 0.0001¥
A-A	25.32	1	25.32	55.02	0.0001
B-B	0.93	1	0.93	2.01	0.199
AB	1.88	1	1.88	4.08	0.0832
A^2	12.05	1	12.05	26.18	0.0014
B^2	17.52	1	17.52	38.07	0.0005
Residual	3.22	7	0.46		
Lack of Fit	1.57	3	0.52	1.26	0.3994£
Pure Error	1.65	4	0.41		
Cor Total	118.74	12			

Where, A: Drug:Polymer ratio (w/w), B: Solvent:Non-Solvent ratio (v/v), ¥ significant and £ not significant

The F-value of a model is 50.21 indicates that it is statistically significant. However, there is just a 0.01% probability that the "F-Value of a model" is this huge might arise because of noise. The estimations of "Prob > F" below 0.10 represents model values are significant. Moreover, in this instance A, B, AB, A^2, B^2 are significant model values. The estimations above 0.10 represents the model values are not significant and the "Lack of Fit F-value" of 1.26 indicates the Lack of Fit is not significant comparative to the pure error. Further, there is a 39.94% possibility that a "Lack of Fit F-value" this huge might arise because of noise.

Table 5.14 Summary of model fitting statistics for % drug loading

Fitting Statistics	
Standard deviation	0.68
Mean	16.29
Coefficient of variance (%)	4.16
PRESS	13.67
R^2	0.9729
Adjusted R^2	0.9535
Predicted R^2	0.8848
Adequate Precision	27.21

The predicted R^2 of 0.8848 is in reasonable concurrence with the adjusted R^2 of 0.9535 (Table 5.14). Adequate precision estimates the signal to noise ratio. Ideally, a ratio more than 4 is desirable. Model ratio of 27.21 represents an adequate signal. Thus, this model might be utilized to explore the design space.

The summary of full quadratic model equations for particle size, PDI and % drug loading were generated by response surface regression process by using design expert software as follows,

Particle size = $+355.408 - 196.75\ A - 1865.09\ B - 345.8\ AB + 536.732\ A^2 + 3537.891\ B^2$

PDI = $+0.218 + 0.016\ A - 0.779\ B - 0.866\ AB + 0.717\ A^2 + 2.261\ B^2$

% drug loading = $+5.805 + 30.972\ A - 9.887\ B - 18.266\ AB - 17.363\ A^2 + 62.651\ B^2$

where, A is drug:polymer ratio (w/w) and B is solvent:non-solvent ratio (v/v)

By clearly examining the coefficient of equations and response surface plots (Fig. 5.4), it shows the particle size, PDI and % drug loading are highly dependent on both the selected independent variables. The positive and negative signs in the polynomial equation suggests the increase and decrease in particle size, PDI and % drug loading with respect to the factor. As there is increase in drug:polymer ratio, increase in the particle size, PDI and % drug loading was noticed. Herein, the quantity of drug was maintained constant by varying in the amount of polymer. From the response surface plots, as the amount of polymer increases resulted in decline in particle size and PDI. This kind of behavior might be due to the excess concentration of hydrophilic moiety (mPEG) as the polymer concentration increases. The role of mPEG in nanoparticle is to act as a capping agent which in turn behaves as a shield on growing particle hence the particle cannot grow after certain extent. When the increase the concentration of mPEG which in turn decreases the average size of

particles and PDI. Moreover, with the increase in drug:polymer ratio, enhancement of % drug loading was observed but above the ratio 0.5 the particle size and PDI got steady increment.

An increase in solvent:non-solvent ratio, the particle size, PDI and % drug loading were found to be decreased till the ratio of 0.25 after that the increase was noticed. This kind of alternations may be because of variation in the viscosity of the dispersion generated during processing. Moreover, higher viscosity of the dispersion by change of solvent:non-solvent ratio leads to more viscous resistance against the shear force during the formation of nanoparticles [52].

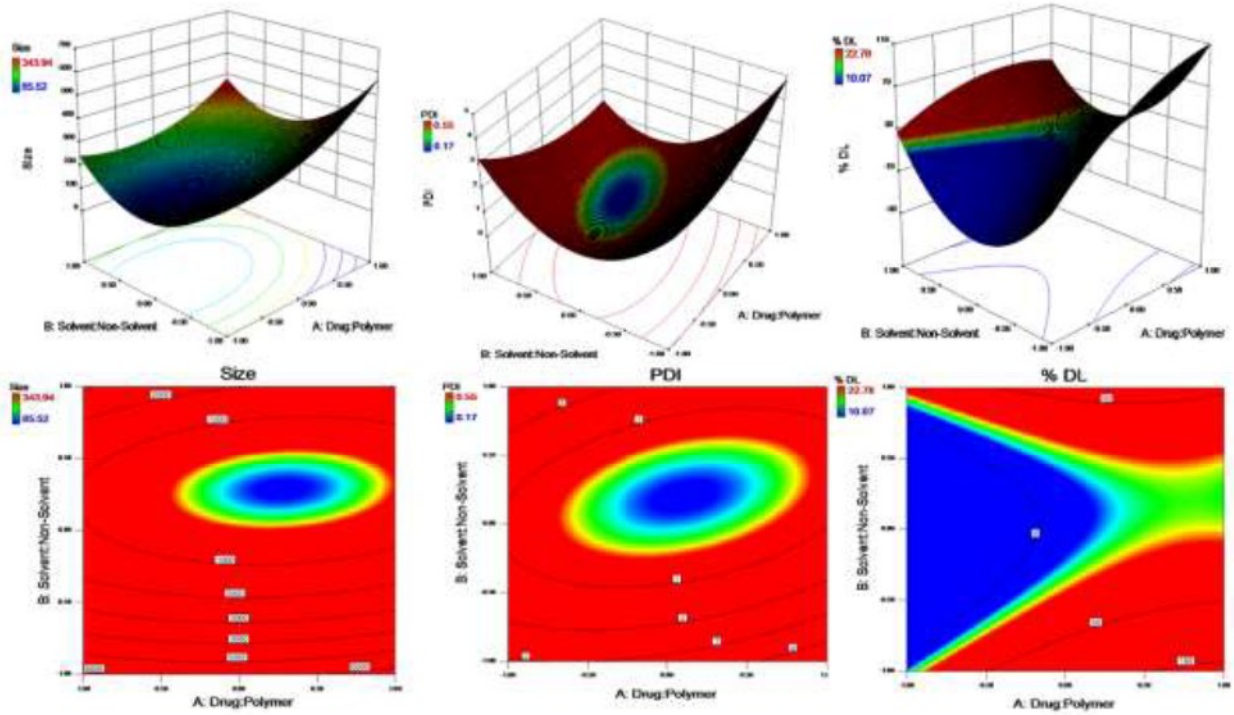

Fig. 5.4 Surface response plots showing the effect of drug:polymer ratio (w/w) and solvent:non-solvent ratio (v/v) on particle size (nm), PDI and % DL, respective sub figures indicate their contour plots

The overlay plot was generated for the prediction of optimized formulation and the independent variables were decided by graphical and numerical approach; thereby optimized formulation was preferred from design space in the overlay plot (Fig. 5.5). Fig. 5.5 defines an overlay plot comprising two sections viz., yellow section represents the optimal design space area with reasonable response and grey section is the area where response does not fit the desired product criteria. The particular criterion for the optimized region was to obtain minimal particle size, PDI and maximal % drug loading. Moreover, the predicted results obtained for the responses like particle size, PDI and % drug loading were validated by comparing them to the actual experimental

values. The differences among the predicted and experimental values were found to be from -6.34 to 5.11. The predicted versus experimental values demonstrated correlation with each other indicating good reliability of the model (Table 5.15).

Table 5.15 Experimental design model validation

Responses	Predicted Values	Experimental Values	% Residuals
Particle size (nm)	100.76	107.15 ± 3.64	-6.34
Polydispersity index	0.22	0.21 ± 0.08	4.55
% Drug loading	17.43	16.54 ± 1.21	5.11

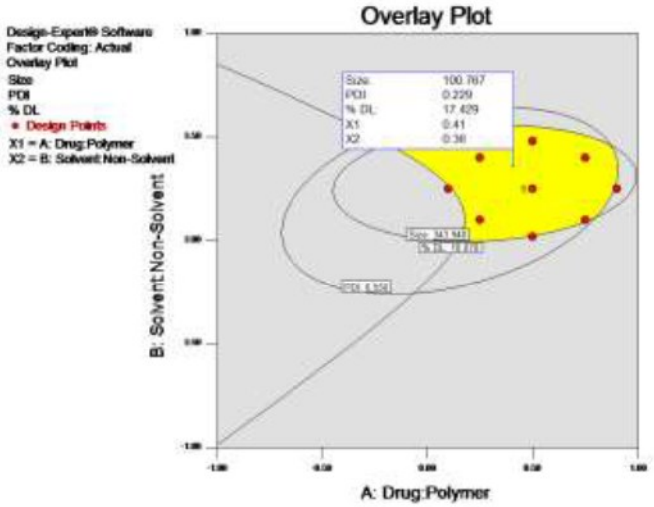

Fig. 5.5 Overlay plot for optimization

We have initially assessed with various cryoprotectants like dextrose, maltose, sucrose and trehalose. Appearance, re-dispersability and size distribution of samples were evaluated and the best results were obtained with trehalose. Further, we have screened the concentration of trehalose and optimized results were obtained with 5% concentration. Redispersibility index was found to be 1.02 ± 0.02 thus we have finalized trehalose with 5% concentration for further studies. The residual content analysis of the organic solvent acetonitrile and triethylamine were estimated by headspace-gas chromatography. As per guidelines acetonitrile belongs to class 2 solvents and triethylamine belongs to class 3 solvents and the content of organic solvent in the lyophilized formulation was found to be below the acceptable limits. The representative chromatograms are shown in Fig. 5.6. The residual organic content of acetonitrile and triethylamine in the lyophilized

polymeric nanoparticles (D1-NPs) was found to be 40.48 ± 9.24 ppm and 24.92 ± 6.51 respectively.

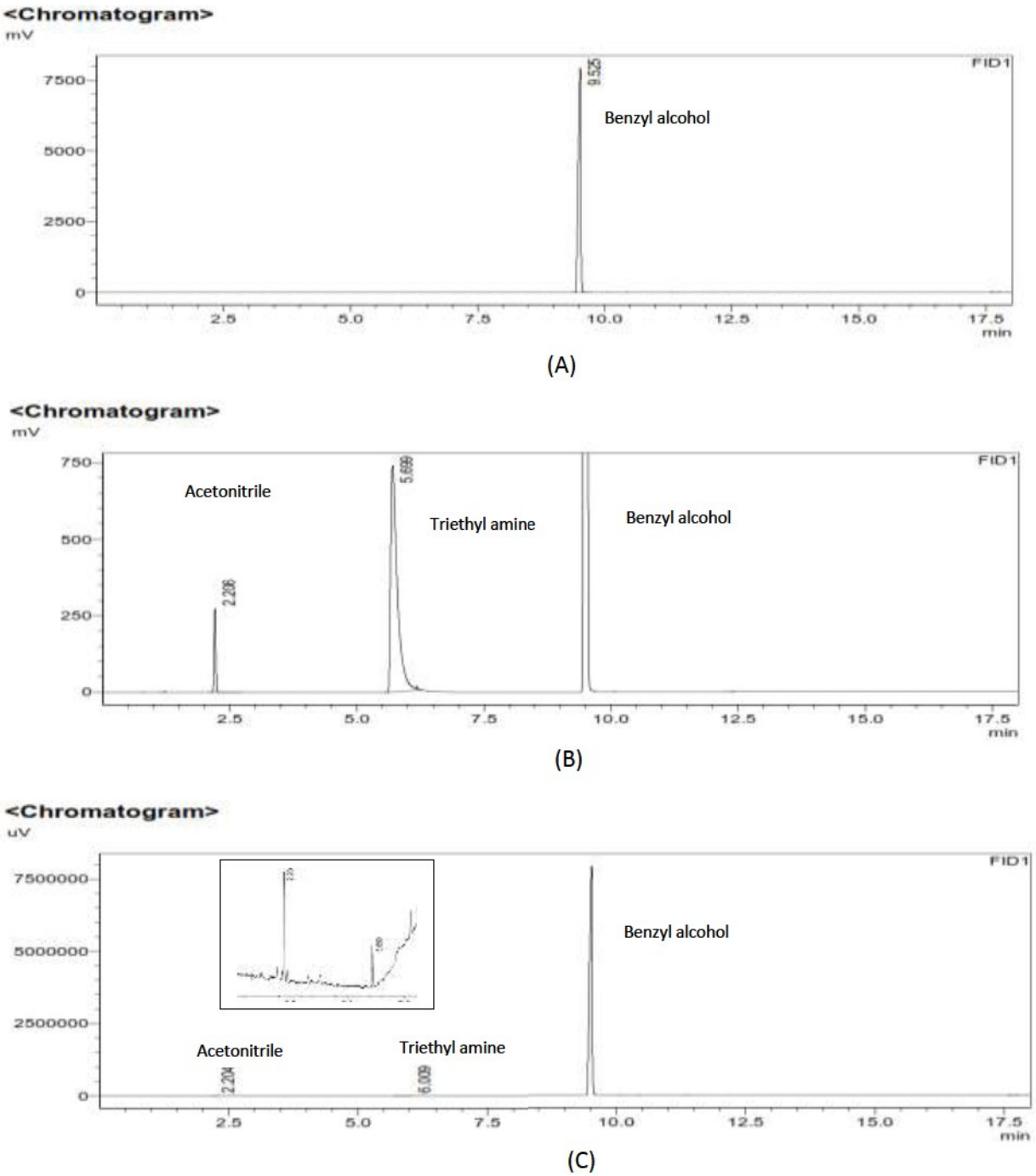

Fig. 5.6 Representative chromatographs for (A) Blank (B) Standard chromatogram spiked with 2000 ppm acetonitrile at Rt: 2.2 min and 5000 ppm trimethyl amine at Rt: 5.6 min (C) Chromatogram for lyophilized polymeric nano-formulation

5.3.3.1 Particle size, zeta potential and morphology

Particle size and its uniform distribution is a pivotal property that has an influence on the drug release pattern, stability and *in-vivo* behavior of the formulation. For target site specific delivery, 50 – 300 nm range is suitable particularly for delivery to the brain. The average particle size, distribution of particles, morphological features and absolute size of the nanoparticles were estimated by FE-SEM and HR-TEM (Fig. 5.7). The polydispersity of the polymeric nanoparticles was found to be 0.24 ± 0.04. The absolute size was found to be in the range of 100-120 nm for both characterization procedures. Moreover, particle morphology has a significant influence on percent drug loading, percent entrapment efficiency, drug release profile, pharmacokinetics and also in biodistribution pattern of the nanoparticles. It also has a role in cellular uptake, cellular internalization, receptor binding and molecular interactions within the cells. The FE-SEM and HR-TEM analysis showed most of the nanoparticles were isometric and the surface was found to be regular. Particle size of these nanoparticles were confirmed by FE-SEM and HR-TEM, it was observed that the absolute size of these particles was lesser than the size represented by DLS. This may be because of measuring mean particle size of nanoparticles by DLS.

Zeta potential (ZP) is the electric potential of the particle movement in a diffusion layer, which is related to slipping or shear plane. Moreover, it is closely associated with stability of the nanoparticles and its surface morphology. It given a key information about the long-term stability of the nano-formulations and their tendency to aggregate. The zeta potential of the polymeric nanoparticles was found to be -6.97 ± 0.99 mV. It indicated the prepared nanoparticle were found to be stable and as for good stability ± 30 mV is desired.

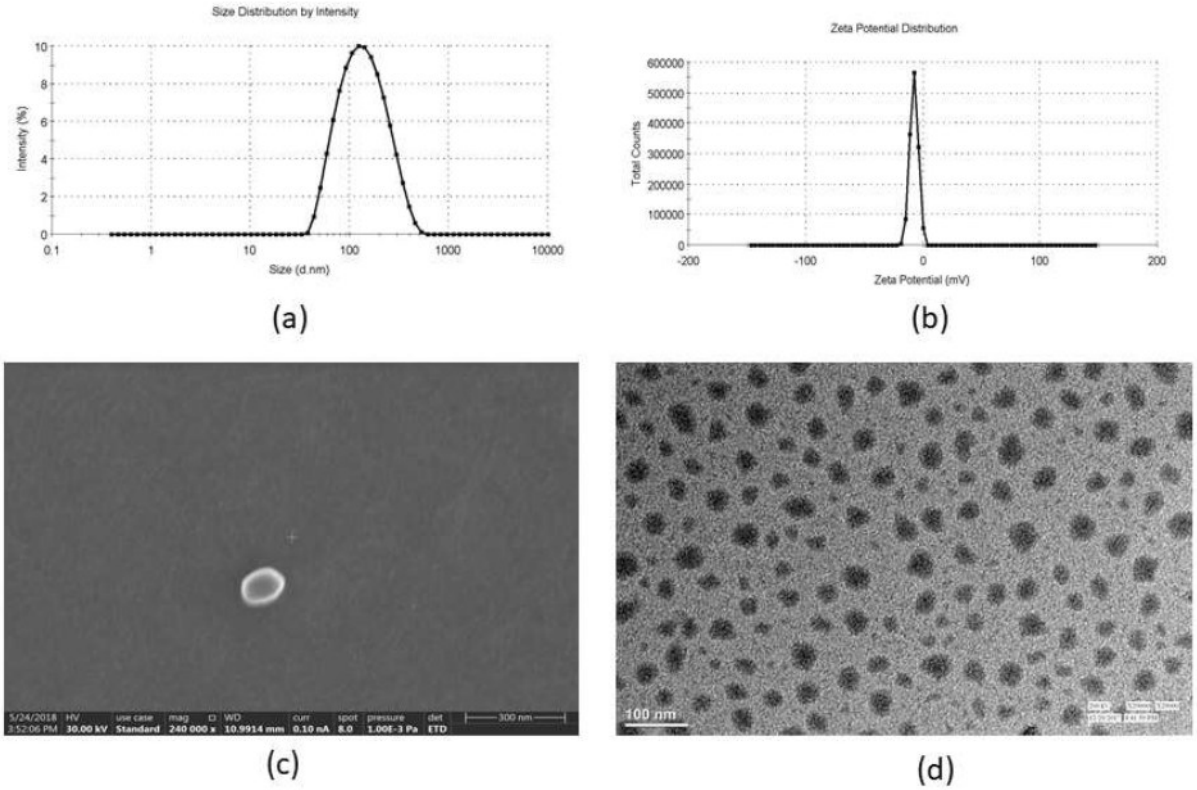

Fig.5.7 Characterization of polymeric nanoparticles by dynamic light scattering (DLS) (a) size, (b) zeta potential, absolute size by (c) FE-SEM and (d) HR-TEM

5.3.4 Surface coating of optimized nanoparticles by polysorbate-80 and ApoE-3 conjugation to the coated nanoparticles

The particle size of D1-NPs before coating was found to be 107.15 ± 1.48 with a zeta potential of 0.79 ± 0.26, while after coating with 1% polysorbate-80 was 124.26 ± 2.19 with a zeta potential of -6.97 ± 0.99. While the D3-NPs showed the particle size of 137.65 ± 2.69 with a zeta potential of -2.08 ± 0.36. The increased particle size of the polymeric nanoparticles conforms coating over the surface. The conjugation efficiency of ApoE3 was found to be 27.21 ± 2.58 %.

5.3.5 Protein binding assay

Protein adsorption plays a pivotal role in stability of nanoparticles in the blood. The nanoparticles with a lipophilic surface have a tendency to adsorb proteins on their surface, which can result in promoting their opsonization and macrophage recognition, thereby increase in the clearance rate leads to elimination from systemic circulation. By utilizing hydrophilic moieties like PEG or poly(ethylene oxide) (PEO), researchers have tried to reduce the protein adsorption of the nanoparticles. PEG and PEO helps in the formation of "stealth" nature to the nanoparticles,

resulting in decreased clearance rate leading to increased blood circulation by restricting interactions with the components of bloodstream [30,53]. These compounds are non-toxic and already grouped as Generally Regarded as Safe (GRAS) by the US-FDA. In this study, we have used PEG in polymeric system, incubated D1-NPs, D2-NPs and D3-NPs with 4% BSA (physiological concentration). The protein adsorption for D1-NPs, D2-NPs and D3-NPs were found to be 4.15 ± 2.12, 3.89 ± 1.79 and 3.59 ± 2.08 % respectively. Due to the existence of PEG units over the surface of nanoparticles resulted in the low protein adsorption, thereby increase in circulation half-life in blood.

5.3.6 *In vitro* drug release studies

The *in vitro* drug release pattern for the nano-formulations were studied utilzing dialysis method, and the drug release profile is shown in Fig. 5.8. DNP loaded nanoparticles observed a biphasic release pattern, an initial burst release within 1 h ~ 40% of drug was released followed by a sustained release pattern till 96 h. It can be concluded from the release studies that the mPEG-PCL nanoparticles exhibit sustained drug release pattern. The sustained drug release from the all the nanoparticles can be ascribed to better encapsulation of drug in the interiors of the nanoparticles, as vivid from percent entrapment studies. To predict the release pattern mechanism, the data was fitted in different mathematical models like zero order, first order, Higuchi, Korsmeyer-Peppas and Hixson-Crowell. Table 5.16 shows the release constants and its regression coefficient values for the respective model. On the basis of regression coefficient values, it is concluded that all the nanoparticles exhibit Korsmeyer-Peppas model with a Fickian diffusion release pattern ($n < 0.43$). This release mechanism might be due to degradation of the nanoparticles, leads to creation of fine pores through which the DNP can be diffused.

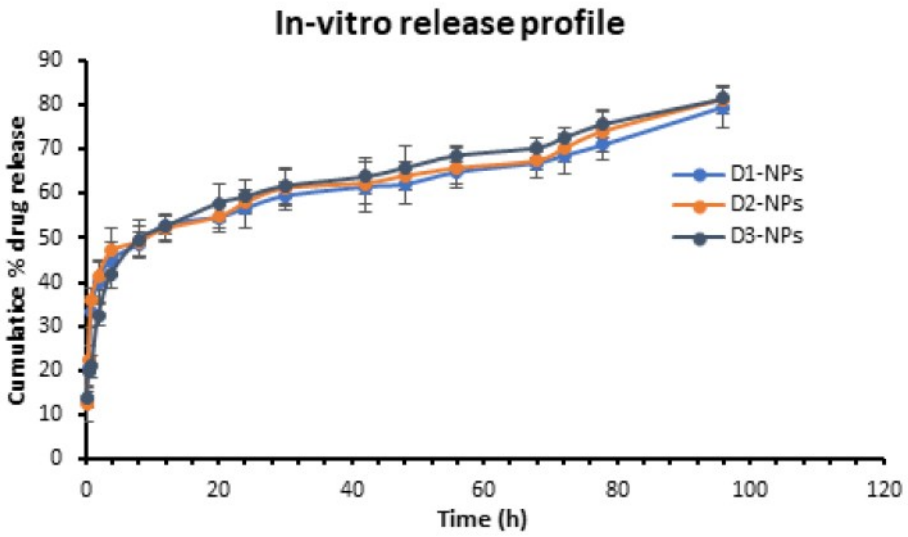

Fig.5.8 In-vitro drug release profile of DNP at pH 7.4 (mean ± SD, n=3)

Table 5.16 Drug release kinetic modeling

Mathematical Modeling	D1-NPs		D2-NPs		D3-NPs	
	Parameters	R^2	Parameters	R^2	Parameters	R^2
Zero Order	K_0: 1.08	0.8598	K_0: 1.11	0.8618	K_0: 0.58	0.8732
First Order	K_1: 0.02	0.9147	K_1: 0.03	0.9130	K_1: 0.03	0.9476
Higuchi	K_H: 9.30	0.9350	K_H: 9.50	0.9326	K_H: 9.67	0.9550
Korsmeyer-Peppas	K_K: 30.27; n: 0.19	0.9735	K_K: 31.14; n: 0.19	0.9688	K_K: 26.87; n: 0.23	0.9871
Hixson-Crowell	K_{HC}: 0.007	0.8996	K_{HC}: 0.007	0.8998	K_{HC}: 0.008	0.9295

5.3.7 Thermal studies

DSC thermogram of polymeric nanoparticles is shown in Fig. 5.9. It has been noticed that, the endothermic peak of DNP in the formulation was not observed indicating that drug was dispersed within the polymer matrix at a molecular level. Disappearance of drug endothermic peak in polymeric nanoparticles has been reported earlier [37].

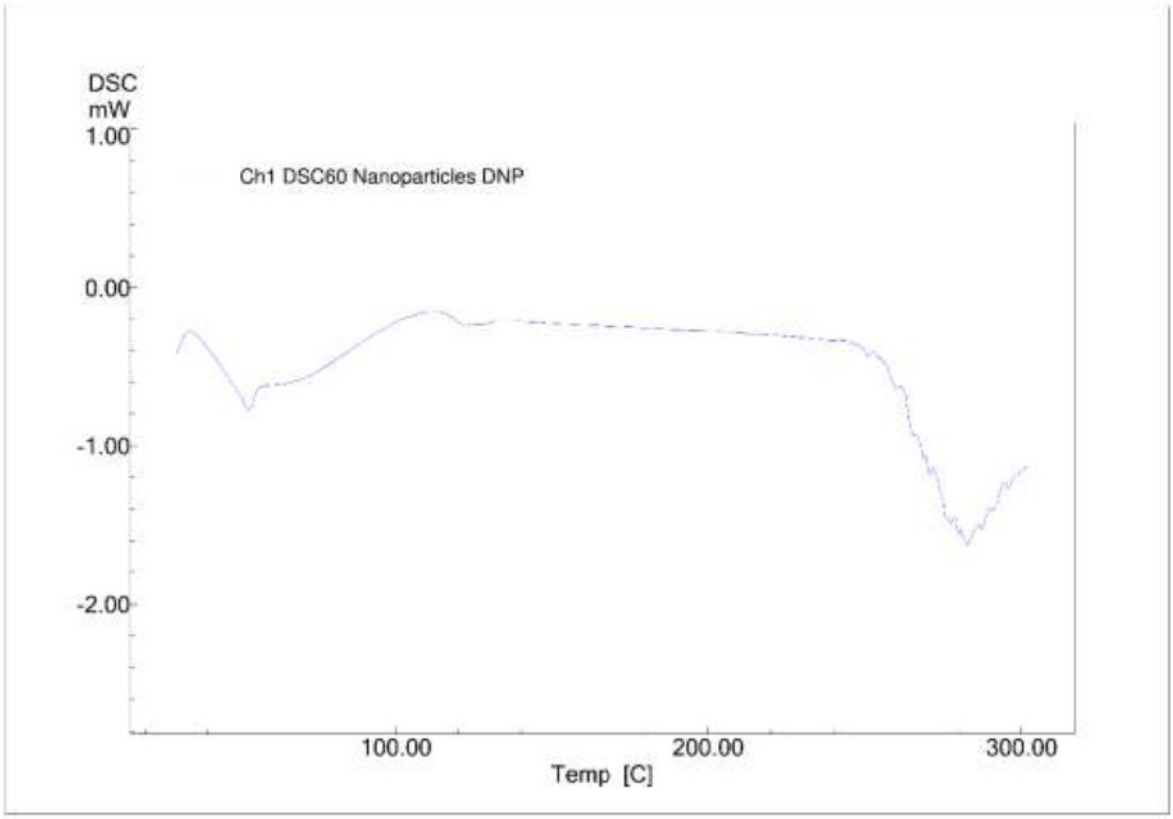

Fig.5.9 DSC thermogram of polymeric nanoparticles

5.3.8 Stability studies

5.3.8.1 Stability of polysorbate-80 coated and Apo-E functionalized polysorbate-80 coated nanoparticles in SGF and SIF:

The influence of simulated biological fluids on particle size, PDI and % EE are shown in Table 5.17. Remarkable differences in particle size, PDI and % EE were detected in D2-NPs due to degradation of the surface coating. Minor difference in particle size, PDI and % EE was noticed in D3-NPs although the changes were insignificant due to the stability of coating in biological fluids. Moreover, it was observed that percentage of surfactant coating remaining in SGF was 89.48 ± 6.4% for D3-NPs and 46.8 ± 5.3% for D2-NPs. Similar pattern was noticed after 6 h of incubation in SIF, where the percentage of coating existing for D3-NPs was found to be 86.54 ± 3.9% and 39.72 ± 5.4% for D2-NPs. These findings suggest that the percentage coating of polysorbate-80 remaining/protected was significantly more in D3-NPs than D2-NPs due to the stability of ApoE3 in gastrointestinal fluids.

Table 5.17 Stability of polymeric nanoparticles in simulated gastric fluids*

Media	Particle Size (nm)				PDI				% EE			
	D2-NPs		D3-NPs		D2-NPs		D3-NPs		D2-NPs		D3-NPs	
	Initial	Final	Initial	Final	Initial	Final	Initial	Final	Initial	Final	Initial	Final
SGF pH 1.2	122.48 ± 2.09	95.12 ± 3.15	138.48 ± 2.94	141.88 ± 1.98	0.17 ± 0.03	0.33 ± 0.12	0.19 ± 0.06	0.22 ± 0.06	90.79 ± 2.91	64.15 ± 3.51	91.09 ± 1.98	88.29 ± 2.15
SIF pH 6.8	122.48 ± 2.09	86.23 ± 2.18	138.48 ± 2.94	143.18 ± 2.33	0.17 ± 0.03	0.45 ± 0.11	0.19 ± 0.06	0.21 ± 0.09	90.79 ± 2.91	59.18 ± 4.39	91.09 ± 1.98	86.18 ± 2.36

*Results were represented as mean ± SD, n=3

5.3.8.2 Long-term stability studies:

The long stability study for nanocarrier delivery system is the major parameter to be considered and should thoroughly characterize its resuspendability. Long-term stability studies were conducted as per the ICH guidelines for all formulations. The particle size, PDI, zeta potential and % EE were evaluated for 3 months, where the formulations were stable and did not show any significant variation in contrast to initial sample (Table 5.18). The log of percent remaining was plotted against time for all the formulations in order to estimate the respective degradation rate (K_{deg}) and $t_{90\%}$ values respectively (Table 5.19). Moreover, lyophilized polymeric nanoparticles showed less than 1 min for redispersion. Thus, the designed lyophilized formulations were found to be stable under various storage conditions.

Table 5.18 Long-term stability studies*

Sampling Time	Long-term Stability Studies (Storage conditions 25 ± 2 °C, 60 ± 5 % RH)											
	size (nm)			PDI			Zeta potential (mV)			% EE		
	D1-NPs	D2-NPs	D3-NPs	D1-NPs	D2-NPs	D3-NPs	D1-NPs	D2-NPs	D3-NPs	D1-NPs	D2-NPs	D3-NPS
initial	107.15 ± 1.48	124.26 ± 2.19	137.65 ± 2.69	0.24 ± 0.04	0.18 ± 0.02	0.21 ± 0.05	0.79 ± 0.26	-6.97 ± 0.99	-2.08 ± 0.36	90.32 ± 2.06	90.79 ± 2.91	90.49 ± 1.98
after 1 month	110.25 ± 2.18	128.15 ± 1.98	141.32 ± 3.65	0.26 ± 0.06	0.21 ± 0.06	0.19 ± 0.07	0.81 ± 0.15	-7.04 ± 1.19	-2.22 ± 0.63	90.04 ± 2.48	90.22 ± 1.95	90.02 ± 2.54
after 2 month	115.18 ± 3.18	131.09 ± 4.12	148.18 ± 2.65	0.25 ± 0.03	0.19 ± 0.04	0.22 ± 0.06	0.72 ± 0.33	-6.88 ± 0.98	-2.49 ± 0.54	88.25 ± 1.94	89.05 ± 2.82	89.19 ± 2.48
after 3 month	114.09 ± 2.41	129.48 ± 3.29	145.17 ± 3.18	0.26 ± 0.04	0.21 ± 0.03	0.23 ± 0.08	0.80 ± 0.19	-7.07 ± 0.89	-2.95 ± 0.71	87.11 ± 2.19	87.27 ± 2.34	87.34 ± 2.73

*Results were represented as mean ± SD, n=3

Table 5.19 Degradation rate kinetic studies for long-term stability data

Formulation	K_{deg} (months^{-1})	$t_{90\%}$ (months)	R^2
D1-NPs	0.0129	8.17	0.9394
D2-NPs	0.0131	8.02	0.9473
D3-NPs	0.0113	9.15	0.9133

5.3.9 Amyloid fibrillation study

The amyloid fibril disintegration study has been performed by utilizing thioflavin-T (ThT) assay. The study demonstrated that, a characteristic sigmoidal curve with a lag phase of 2 h and a plateau observed at 24 h for the $A\beta_{1-42}$ aggregation process (Fig. 5.10). The lag phase gives information about the nucleation phase of the $A\beta_{1-42}$ aggregation process, whereas the plateau represents the development of matured and well aggregated β-sheet-rich $A\beta_{1-42}$ fibrils. No significant changes in the lag phase was observed when 50 µg/mL DNP and its formulations were co-incubated with 25 µM $A\beta_{1-42}$, but the plateau formation was decreased significantly in case of D3-NPs. Further, all the formulations exhibited lower fluorescence signal with respect to the $A\beta_{1-42}$ solution. ThT signal has been decreased in the presence of pure drug, D1-NPs and D2-NPs but cannot significantly inhibit $A\beta_{1-42}$ fibril formation. Fibrillation rate kinetic derived parameters by fitting ThT data are shown in Table 5.20. D3-NPs were able to interfere at all stages of aggregation procedure by decreasing the aggregation lag phase and fibrillation growth rate.

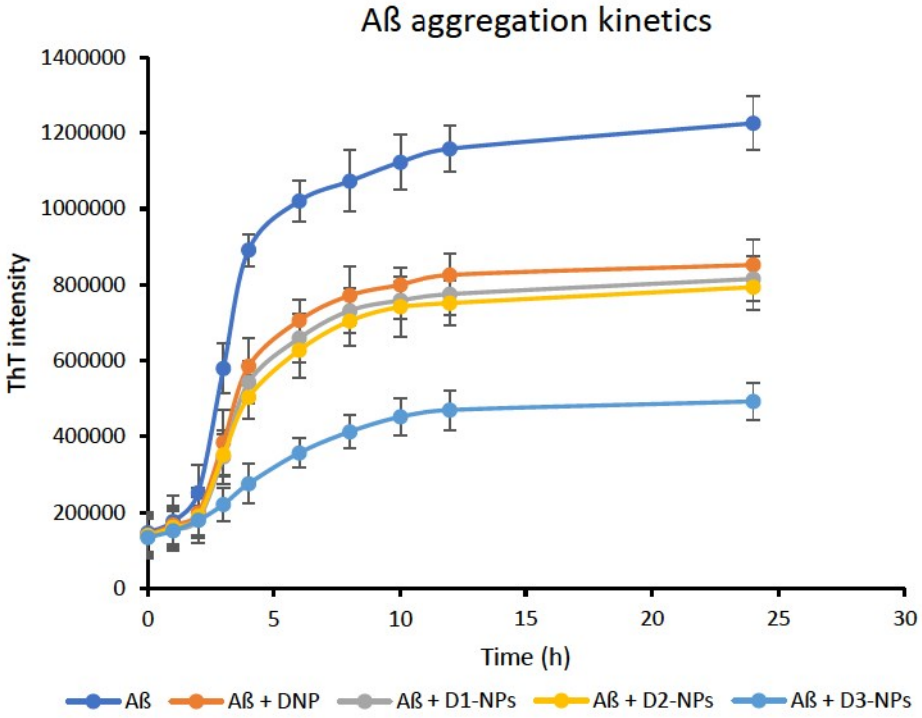

Fig. 5.10 $A\beta_{1-42}$ aggregation kinetics

Table 5.20 Fibrillation rate kinetic parameters derived by fitting ThT data

Group	t_0 (h)	t_{lag} (h)	K_{fib} (1/h)	Y_f (%)
$A\beta_{1-42}$	3.18	1.73	1.38	100.00
$A\beta_{1-42}$ + DNP	3.43	1.41	0.99	71.03
$A\beta_{1-42}$ + D1-NPs	3.54	1.42	0.94	66.75
$A\beta_{1-42}$ + D2-NPs	3.56	0.72	0.70	64.91
$A\beta_{1-42}$ + D3-NPs	4.21	0.16	0.41	41.13

5.2.9.1 Proteolysis assay

Proteolysis assay was performed to explore the enzymatic degradation rate of Aβ fibrils and mixture of Aβ fibrils with pure drug, D1-NPs, D2-NPs and D3-NPs (Fig. 5.11). After incubation of Aβ fibrils with proteinase K, the ThT florescence intensity was decreased after 3 h and later increased to the initial levels. This sort of phenomenon may be due to mature Aβ fibrils were not degraded by proteolysis. Samples treated with pure drug, D1-NPs, D2-NPs and D3-NPs exhibited decreased florescence intensity with respect to time. However, a significant drop in ThT florescence intensity was detected in samples treated with D3-NPs, may be due to surface functionalization of ApoE3. These results indicate that D3-NPs were able to boost the process of degradation of Aβ aggregates, that is necessary for maintenance of Aβ homeostasis [48].

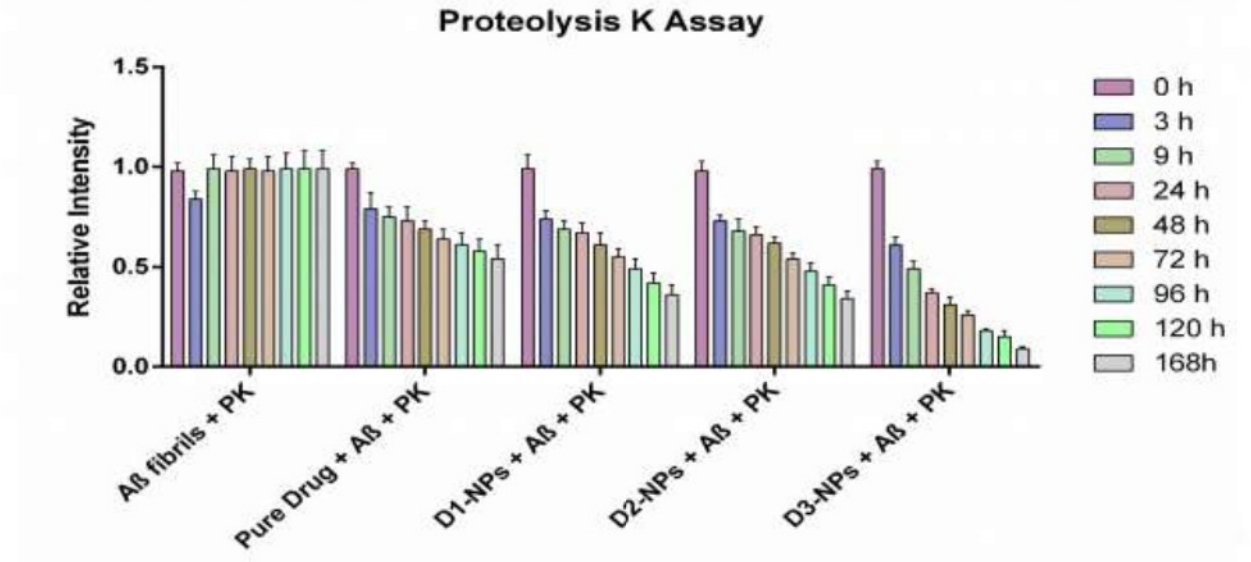

Fig. 5.11 Degradation effect of amyloid fibrils with pure drug and its formulations complexes by proteinase K using ThT fluorescence assay

5.2.10 Cell culture studies

(a) Cell viability assay

The cytotoxicity of pure drug and nanoparticles were estimated in the HepG2, U-87 and SHSY-5Y cells utilizing the MTT cytotoxicity assay. The MTT assay evaluates cellular oxidative metabolic activity depending on the activity of NAD(P)H-dependent dehydrogenase enzymes. The effect of various concentrations (50-500µg/mL) of DNP on the viability of HepG2**,** U-87 and SHSY-5Y cells (Fig. 5.12) were explored. The cell viability above ~ 85-90% in the concentration range 50-150µg/mL, indicates the biocompatibility and nontoxicity of the polymeric nanoparticles. However, DNP showed 50-60% cell viability in HepG2 cells and 60-70% viable cells in both U87 and SHSY-5Y cell lines at the concentration range 300-500µg/mL, whereas DNP polymeric nanoparticles showed slightly less cytotoxicity in all the cell lines. These results represent that the DNP polymeric nanoparticles are biocompatible in the concentration range 50-500µg/mL and can further be utilized at slightly higher concentrations and thus are suitable as drug carriers.

(b) Cellular uptake studies

D3-NPs showed significantly higher uptake in both neuronal cell lines. It was observed that nearly about 85.96 ± 1.86 % uptake in U87 cells, while in case of SHSY-5Y it was about 88.48 ± 2.71 %. The higher uptake in both these cell lines might be due to its nanosize and surface modifications is the added advantage in D3-NPs for active targeting (Fig. 5.13).

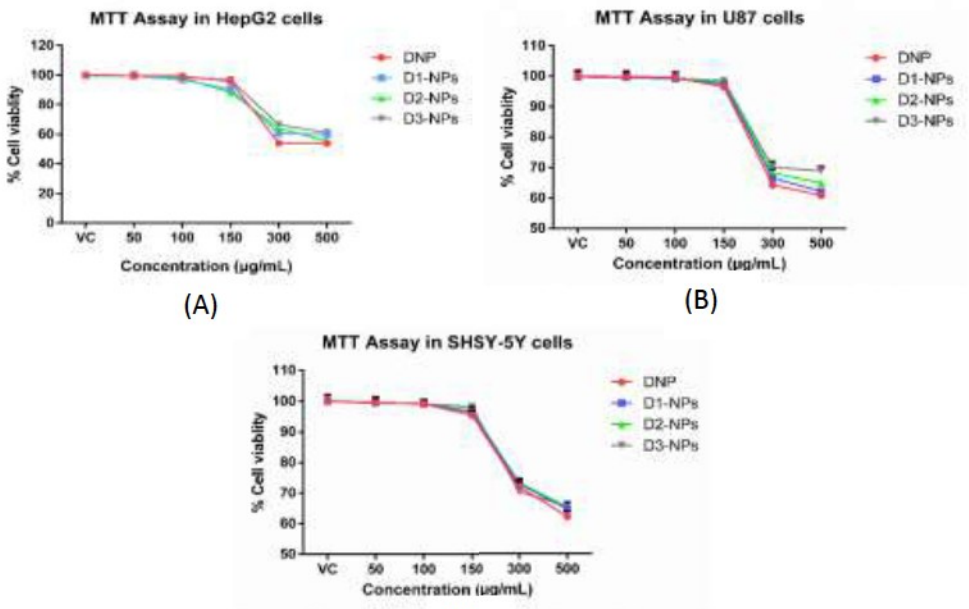

Fig. 5.12 MTT assay of nanoparticles in (A) HepG2 (B) U87 and (C) SHSY-5Y cell lines

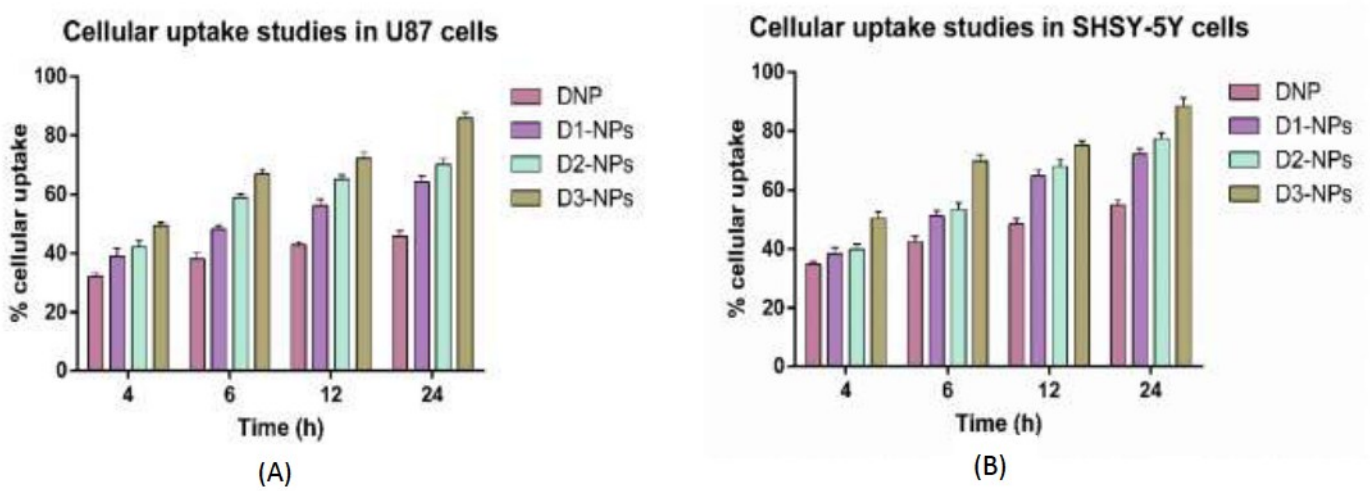

Fig.5.13 Cellular uptake studies in (A) U87 cells and (B) SHSY-5Y cells

(c) Amyloid beta$_{1-42}$ induced neuronal toxicity in cell lines

The influence of $A\beta_{1-42}$ fibril aggregates on the SH-SY5Y human neuroblastoma cells was estimated using cell viability assay. In the experimentation process, the value obtained for cell media existing with SH-SY5Y cells was considered as 100 % viable cells. Further, the $A\beta_{1-42}$ peptide was permitted to oligomerize and fibrillize for about 24 h in the same cell culture media. The obtained solution was added to the SH-SY5Y containing wells. The viability of cells decreased to 35 ± 3% of the control, representing that $A\beta_{1-42}$ oligomers and fibrils are cytotoxic in nature. Although, when $A\beta_{1-42}$ was co-incubated with pure drug, D1-NPs, D2-NPs and D3-NPs for 24 h, the cell viability was rescued to 58 ± 3% at 50µg/mL and 64 ± 4 at 150 µg/mL (Fig. 5.14). Higher cell viability was obtained when cells were treated with D3-NPs at both concentrations which indicates the improved efficiency of the formulation by clearing the $A\beta_{1-42}$ fibrils due to the existence of ApoE3 peptide over the surface of the nanoparticles. Moreover, in the *in vivo* conditions $A\beta_{1-42}$ peptides exist at nanomolar range, which is significantly less than micromolar concentrations utilized for *in vitro* aggregate formation. Indeed, we found that in case of D3-NPs the toxicity was abolished because of surface functionalization.

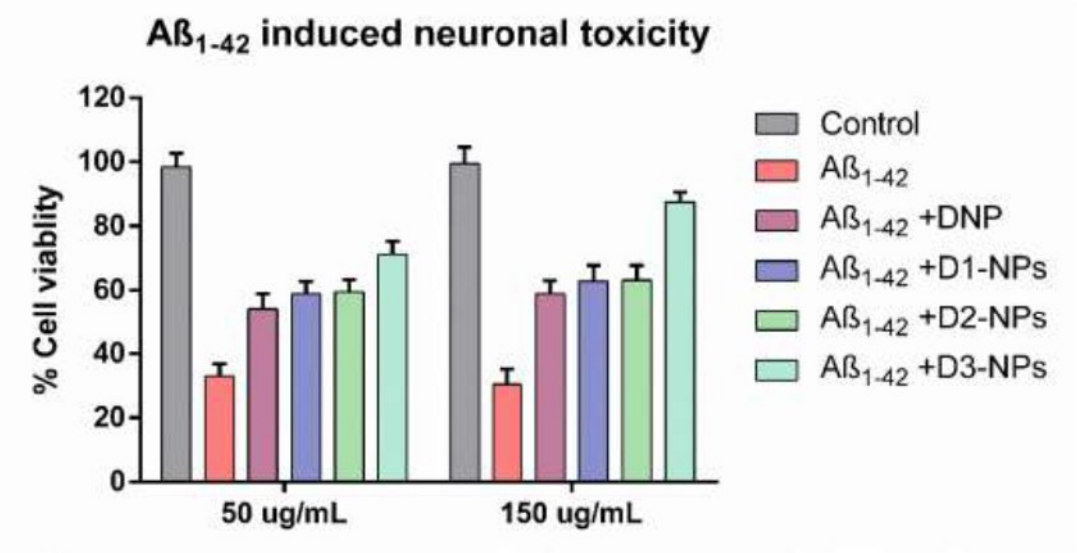

Fig. 5.14 SHSY-5Y cellular viability after being exposed to $A\beta_{1-42}$ fibrils

Conclusions

Amphiphilic di-block copolymers were successfully synthesized and thoroughly characterized by using ^{1}HNMR, GPC and FTIR. Donepezil loaded nanoparticles were fabricated as polymeric nanoparticles using in-house synthesized mPEG-PCL di-block polymer. Different preparation techniques like film hydration, solvent evaporation, nanoprecipitation methods have been screened to achieve maximum drug loading and entrapment efficacy without compromising on size of the nanoparticles. Nanoprecipitation technique has shown better results in comparison with other methods with below < 200 nm with good drug loading and extended release. The influence of formulation variables like drug:polymer ratio (w/w) and solvent:non-solvent ratio (v/v) on particle size, polydispersity index and percent drug loading were studied in detail using Design-Expert software. The lyophilized nanoparticles showed good redispersibility index and the organic content was estimated by using GC-HS. SEM and TEM analysis exhibited that the particles were isometric in shape and with regular surface. Extended release of these nano-formulations has been observed in *in vitro* studies. The *in vitro* data in simulated gastric fluids suggested that polysorbate 80 coating was found to be stable in ApoE3 coated nanoparticles and the concentration of polysorbate 80 remaining on the surface was in agreement with the initial coating amount. Moreover, it has been observed that, ApoE3 conjugated polymeric nanoparticles efficiently interferes at all steps of Aβ aggregation kinetics *in vitro*, which was confirmed by thioflavin t assay. All the formulations were found to be non-cytotoxic and biocompatible in neuroblastoma

and liver cell lines and ApoE3 conjugated polymeric nanoparticles were able to attenuate $A\beta_{1-42}$ induced cytotoxicity in SHSY-5Y cells. Further, to establish the suitability of these nano-formulations as a potential carrier system, the optimized formulations were further evaluated for *in-vivo* pharmacokinetic, bio-distribution and pharmacodynamic studies.

References

[1] W.A. Banks, From blood--brain barrier to blood--brain interface: new opportunities for CNS drug delivery, Nat. Rev. Drug Discov. 15 (2016) 275.

[2] M.D. Sweeney, Z. Zhao, A. Montagne, A.R. Nelson, B. V Zlokovic, Blood-brain barrier: from physiology to disease and back, Physiol. Rev. 99 (2019) 21–78.

[3] S. Bergmann, S.E. Lawler, Y. Qu, C.M. Fadzen, J.M. Wolfe, M.S. Regan, B.L. Pentelute, N.Y.R. Agar, C.-F. Cho, Blood--brain-barrier organoids for investigating the permeability of CNS therapeutics, Nat. Protoc. 13 (2018) 2827–2843.

[4] M.M. Wen, N.S. El-Salamouni, W.M. El-Refaie, H.A. Hazzah, M.M. Ali, G. Tosi, R.M. Farid, M.J. Blanco-Prieto, N. Billa, A.S. Hanafy, Nanotechnology-based drug delivery systems for Alzheimer's disease management: Technical, industrial, and clinical challenges, J. Control. Release. 245 (2017) 95–107.

[5] G. Sharma, A.R. Sharma, S.-S. Lee, M. Bhattacharya, J.-S. Nam, C. Chakraborty, Advances in nanocarriers enabled brain targeted drug delivery across blood brain barrier, Int. J. Pharm. (2019).

[6] K.R. Gajbhiye, A. Pawar, K.R. Mahadik, V. Gajbhiye, PEGylated Nanocarriers: A Promising Tool for Targeted Delivery to the Brain, Colloids Surfaces B Biointerfaces. (2020) 110770.

[7] S. Parvaz, R. Taheri-Ledari, M.S. Esmaeili, M. Rabbani, A. Maleki, A brief survey on the advanced brain drug administration by nanoscale carriers: With a particular focus on AChE reactivators, Life Sci. 240 (2020) 117099.

[8] N. Poovaiah, Z. Davoudi, H. Peng, B. Schlichtmann, S. Mallapragada, B. Narasimhan, Q. Wang, Treatment of neurodegenerative disorders through the blood--brain barrier using nanocarriers, Nanoscale. 10 (2018) 16962–16983.

[9] X. Niu, J. Chen, J. Gao, Nanocarriers as a powerful vehicle to overcome blood-brain barrier in treating neurodegenerative diseases: Focus on recent advances, Asian J. Pharm. Sci. 14 (2019) 480–496.

[10] M. Agrawal, S. Saraf, S. Saraf, S.G. Antimisiaris, N. Hamano, S.-D. Li, M. Chougule, S.A. Shoyele, U. Gupta, Ajazuddin, others, Recent advancements in the field of nanotechnology for the delivery of anti-Alzheimer drug in the brain region, Expert Opin. Drug Deliv. 15 (2018) 589–617.

[11] G. Karthivashan, P. Ganesan, S.-Y. Park, J.-S. Kim, D.-K. Choi, Therapeutic strategies and nano-drug delivery applications in management of ageing Alzheimer's disease, Drug Deliv. 25 (2018) 307–320.

[12] D. Gopalan, A. Pandey, N. Udupa, S. Mutalik, Receptor specific, stimuli responsive and subcellular targeted approaches for effective therapy of Alzheimer: Role of surface engineered nanocarriers, J. Control. Release. 319 (2020) 183–200.

[13] M. Dooley, H.M. Lamb, Donepezil, Drugs Aging. 16 (2000) 199–226.

[14] E.Y. Shintani, K.M. Uchida, Donepezil: an anticholinesterase inhibitor for Alzheimer's disease, Am. J. Heal. Pharm. 54 (1997) 2805–2810.

[15] Q. Song, M. Huang, L. Yao, X. Wang, X. Gu, J. Chen, J. Chen, J. Huang, Q. Hu, T. Kang, others, Lipoprotein-based nanoparticles rescue the memory loss of mice with Alzheimer's disease by accelerating the clearance of amyloid-beta, ACS Nano. 8 (2014) 2345–2359.

[16] S. Wagner, A. Zensi, S.L. Wien, S.E. Tschickardt, W. Maier, T. Vogel, F. Worek, C.U. Pietrzik, J. Kreuter, H. Von Briesen, Uptake mechanism of ApoE-modified nanoparticles on brain capillary endothelial cells as a blood-brain barrier model, PLoS One. 7 (2012) e32568.

[17] M.A. Arya, M.K.M. Kumar, M. Sabitha, K.K. Menon, S.C. Nair, Nanotechnology approaches for enhanced CNS delivery in treating Alzheimer's disease, J. Drug Deliv. Sci. Technol. (2019).

[18] H. Derakhshankhah, S. Sajadimajd, S. Jafari, Z. Izadi, S. Sarvari, M. Sharifi, M. Falahati, F. Moakedi, W.C.A. Muganda, M. Müller, others, Novel therapeutic strategies for Alzheimer's disease: Implications from cell-based therapy and Nanotherapy, Nanomedicine Nanotechnology, Biol. Med. (2020) 102149.

[19] S. Tiwari, V. Atluri, A. Kaushik, A. Yndart, M. Nair, Alzheimer's disease: pathogenesis, diagnostics, and therapeutics, Int. J. Nanomedicine. 14 (2019) 5541.

[20] P. Zhang, L. Chen, W. Gu, Z. Xu, Y. Gao, Y. Li, In vitro and in vivo evaluation of donepezil-sustained release microparticles for the treatment of Alzheimer's disease, Biomaterials. 28 (2007) 1882–1888.

[21] W. Guo, P. Quan, L. Fang, D. Cun, M. Yang, Sustained release donepezil loaded PLGA microspheres for injection: Preparation, in vitro and in vivo study, Asian J. Pharm. Sci. 10 (2015) 405–414.

[22] I. Baysal, G. Ucar, M. Gultekinoglu, K. Ulubayram, S. Yabanoglu-Ciftci, Donepezil loaded PLGA-b-PEG nanoparticles: their ability to induce destabilization of amyloid fibrils and to cross blood brain barrier in vitro, J. Neural Transm. 124 (2017) 33–45.

[23] D. Brambilla, R. Verpillot, B. Le Droumaguet, J. Nicolas, M. Taverna, J. Kóňa, B. Lettiero, S.H. Hashemi, L. De Kimpe, M. Canovi, others, PEGylated nanoparticles bind to and alter amyloid-beta peptide conformation: toward engineering of functional nanomedicines for Alzheimer's disease, ACS Nano. 6 (2012) 5897–5908.

[24] S. Zamani, S. Khoee, Preparation of core--shell chitosan/PCL-PEG triblock copolymer nanoparticles with ABA and BAB morphologies: Effect of intraparticle interactions on physicochemical properties, Polymer (Guildf). 53 (2012) 5723–5736.

[25] W. Peng, X. Jiang, Y. Zhu, E. Omari-Siaw, W. Deng, J. Yu, X. Xu, W. Zhang, Oral delivery of capsaicin using MPEG-PCL nanoparticles, Acta Pharmacol. Sin. 36 (2015) 139.

[26] C.I.C. Crucho, M.T. Barros, Polymeric nanoparticles: A study on the preparation variables and characterization methods, Mater. Sci. Eng. C. 80 (2017) 771–784.

[27] D. Bennet, S. Kim, Polymer nanoparticles for smart drug delivery, chapter, 2014.

[28] M. Munjal, Nanoparticles-Preparation, technology, evaluation and used in targeted drug delivery system, Technology. 14 (2018) 15.

[29] B.L. Banik, P. Fattahi, J.L. Brown, Polymeric nanoparticles: the future of nanomedicine, Wiley Interdiscip. Rev. Nanomedicine Nanobiotechnology. 8 (2016) 271–299.

[30] C. Nehate, A.A. Moothedathu Raynold, V. Haridas, V. Koul, Comparative Assessment of Active Targeted Redox Sensitive Polymersomes Based on pPEGMA-S-S-PLA Diblock Copolymer with Marketed Nanoformulation, Biomacromolecules. (2018) acs.biomac.8b00178. doi:10.1021/acs.biomac.8b00178.

[31] C. Nehate, A.A. Moothedathu Raynold, V. Koul, ATRP fabricated and short chain polyethylenimine grafted redox sensitive polymeric nanoparticles for codelivery of anticancer drug and siRNA in cancer therapy, ACS Appl. Mater. Interfaces. 9 (2017) 39672–39687.

[32] O.M. Saka, U.C. Öz, B. Küçüktürkmen, B. Devrim, A. Bozk\ir, Central composite design for optimization of zoledronic acid loaded PLGA nanoparticles, J. Pharm. Innov. (2018) 1–12.

[33] U.C. Oz, B. Küçüktürkmen, B. Devrim, O.M. Saka, A. Bozkir, Development and

Optimization of Alendronate Sodium Loaded PLGA Nanoparticles by Central Composite Design, Macromol. Res. 27 (2019) 857–866.

[34] G. Mittal, H. Carswell, R. Brett, S. Currie, M.N.V.R. Kumar, Development and evaluation of polymer nanoparticles for oral delivery of estradiol to rat brain in a model of Alzheimer's pathology, J. Control. Release. 150 (2011) 220–228.

[35] B. Wilson, M.K. Samanta, K. Santhi, K.P.S. Kumar, N. Paramakrishnan, B. Suresh, Targeted delivery of tacrine into the brain with polysorbate 80-coated poly (n-butylcyanoacrylate) nanoparticles, Eur. J. Pharm. Biopharm. 70 (2008) 75–84.

[36] B. Wilson, M.K. Samanta, K. Santhi, K.P.S. Kumar, N. Paramakrishnan, B. Suresh, Poly (n-butylcyanoacrylate) nanoparticles coated with polysorbate 80 for the targeted delivery of rivastigmine into the brain to treat Alzheimer's disease, Brain Res. 1200 (2008) 159–168.

[37] E. Joseph, S. Reddi, V. Rinwa, G. Balwani, R. Saha, DoE based Olanzapine loaded poly-caprolactone nanoparticles decreases extrapyramidal effects in rodent model, Int. J. Pharm. 541 (2018) 198–205.

[38] R.S. Mulik, J. Mönkkönen, R.O. Juvonen, K.R. Mahadik, A.R. Paradkar, ApoE3 mediated poly (butyl) cyanoacrylate nanoparticles containing curcumin: study of enhanced activity of curcumin against beta amyloid induced cytotoxicity using in vitro cell culture model, Mol. Pharm. 7 (2010) 815–825.

[39] R.S. Mulik, J. Mönkkönen, R.O. Juvonen, K.R. Mahadik, A.R. Paradkar, ApoE3 mediated polymeric nanoparticles containing curcumin: apoptosis induced in vitro anticancer activity against neuroblastoma cells, Int. J. Pharm. 437 (2012) 29–41.

[40] M.M. Bradford, A rapid and sensitive method for the quantitation of microgram quantities of protein utilizing the principle of protein-dye binding, Anal. Biochem. 72 (1976) 248–254.

[41] V. Hlady, J. Buijs, H.P. Jennissen, Methods for studying protein adsorption, in: Methods Enzymol., Elsevier, 1999: pp. 402–429.

[42] K.V. Krishna, R.N. Saha, G. Singhvi, S.K. Dubey, Pre-clinical pharmacokinetic-pharmacodynamic modelling and biodistribution studies of donepezil hydrochloride by a validated HPLC method, RSC Adv. 8 (2018) 24740–24749.

[43] E. Nemutlu, \.Ipek Ero\uglu, H. Ero\uglu, S. K\ir, In Vitro Release Test of Nano-Drug Delivery Systems Based on Analytical and Technological Perspectives, Curr. Anal. Chem.

15 (2019) 373–409.

[44] S. Dash, P.N. Murthy, L. Nath, P. Chowdhury, others, Kinetic modeling on drug release from controlled drug delivery systems, Acta Pol Pharm. 67 (2010) 217–223.

[45] K.H. Ramteke, P.A. Dighe, A.R. Kharat, S. V Patil, Mathematical models of drug dissolution: a review, Sch. Acad. J. Pharm. 3 (2014) 388–396.

[46] H.T.G. ICH, Stability testing of new drug substances and products Q1A (R2), in: Proc. Int. Conf. Harmon. Geneva, 2003.

[47] H. Zhou, Z. Yang, X. Tian, L. Chen, S. Lee, T. Huynh, C. Ge, R. Zhou, Lanosterol disrupts the aggregation of amyloid-β peptides, ACS Chem. Neurosci. 10 (2019) 4051–4060.

[48] F. Huang, A. Qu, H. Yang, L. Zhu, H. Zhou, J. Liu, J. Long, L. Shi, Self-Assembly Molecular Chaperone to Concurrently Inhibit the Production and Aggregation of Amyloid β Peptide Associated with Alzheimer's Disease, ACS Macro Lett. 7 (2018) 983–989.

[49] B. Le Droumaguet, J. Nicolas, D. Brambilla, S. Mura, A. Maksimenko, L. De Kimpe, E. Salvati, C. Zona, C. Airoldi, M. Canovi, others, Versatile and efficient targeting using a single nanoparticulate platform: application to cancer and Alzheimer's disease, ACS Nano. 6 (2012) 5866–5879.

[50] M. Li, X. Yang, J. Ren, K. Qu, X. Qu, Using graphene oxide high near-infrared absorbance for photothermal treatment of Alzheimer's disease, Adv. Mater. 24 (2012) 1722–1728.

[51] W. Wu, X. Sun, Y. Yu, J. Hu, L. Zhao, Q. Liu, Y. Zhao, Y. Li, TiO2 nanoparticles promote β-amyloid fibrillation in vitro, Biochem. Biophys. Res. Commun. 373 (2008) 315–318.

[52] K.V. Krishna, G. Wadhwa, A. Alexander, N. Kanojia, R.N. Saha, R. Kukreti, G. Singhvi, S.K. Dubey, Design and biological evaluation of lipoprotein-based donepezil nanocarrier for enhanced brain uptake through oral delivery, ACS Chem. Neurosci. 10 (2019) 4124–4135.

[53] P. Calvo, B. Gouritin, H. Chacun, D. Desmaële, J. D'Angelo, J.-P. Noel, D. Georgin, E. Fattal, J.P. Andreux, P. Couvreur, Long-circulating PEGylated polycyanoacrylate nanoparticles as new drug carrier for brain delivery, Pharm. Res. 18 (2001) 1157–1166.